

Institut für Angewandte Physik
der Universität Bonn

Wegelerstraße 8
53115 Bonn

A high finesse optical resonator for cavity QED experiments

von
Wenjamin Rosenfeld

Diplomarbeit in Physik

angefertigt im
Institut für Angewandte Physik

vorgelegt der
Mathematisch-Naturwissenschaftlichen Fakultät
der Rheinischen Friedrich-Wilhelms-Universität
Bonn
im August 2003

Referent: Prof. Dr. D. Meschede
Korreferent: Prof. Dr. K. Buse

Contents

Introduction	4
1 Theory	6
1.1 Optical resonators	6
1.1.1 Basic properties	6
1.1.2 Eigenmodes	8
1.1.3 Quantization of the electromagnetic field	10
1.1.4 Photon lifetime	11
1.2 Atom-cavity interaction	12
1.2.1 Atom-cavity coupling strength	12
1.2.2 Jaynes-Cummings model	12
1.2.3 Dissipation and strong coupling	14
1.2.4 Density matrix approach	14
1.2.5 Interaction between two atoms	18
2 Cavity setup	19
2.1 Resonator assembly	19
2.1.1 High reflectivity mirrors	19
2.1.2 Assembly	21
2.2 Characterization of the cavity	23
2.2.1 Voltage-travel relation of piezo elements	25
2.2.2 Resonator length	25
2.2.3 Cavity linewidth and finesse	27
2.2.4 Resulting parameters	28
2.3 Single-atoms setup	29
2.3.1 Single-atom MOT	29
2.3.2 Optical conveyor belt	30
2.3.3 Manipulation and measurement of internal states	31
2.3.4 Integration of the cavity into current setup	32
2.4 Conclusion	34

3	Active stabilization of the cavity	35
3.1	Pound-Drever-Hall method	35
3.2	Stabilization setup	38
3.3	Improvement of the stabilization system	39
3.3.1	Compensation of resonances	40
3.3.2	Resonantly amplified APD	42
3.4	Performance of the stabilization system	43
3.4.1	Characterization of the chain of locks	43
3.4.2	Scanning of the stabilized cavity	45
3.5	Conclusion	45
4	Cavity ring-down	47
4.1	Basic principle	47
4.2	Setup	48
4.2.1	Mirror holder	49
4.2.2	Laser switching	50
4.3	Measurements	51
4.3.1	Procedure	51
4.3.2	Analysis	52
4.3.3	Precision limits and reproducibility	53
4.3.4	Characterization of a mirror set	54
	Summary and outlook	56
	A Solution of the master equation	57
	Bibliography	59

Introduction

The idea of quantum information processing attracted much attention in recent years. A quantum computer works with qubits, which, as opposed to classical bits with only two defined states, are any coherent superposition of two states. Quantum computing opens a new range of possibilities, especially parallel processing of information. Recently developed quantum algorithms [Shor94] show that quantum computers can solve specific problems within polynomial time for which classical computers take exponential time.

The experimental realization of such systems, however, encounters severe technical problems. First, one must be able to control quantum systems. Some examples which are related to our field are ions [Lieb03], neutral atoms, even “artificial” atoms (quantum dots). Besides the experimental challenge to store them, we need to control their quantum states. Here, the greatest difficulty is the preservation of quantum coherence. Any coherent superposition of states must last much longer than the computation time. This means that the dissipation and thus the interaction with the environment must be suppressed. The charge of the ions leads to Coulomb interaction with the environment which quickly destroys the coherence. Quantum dots are incorporated into solid material and suffer the same problem.

Our experiment is an approach to an implementation using individual neutral atoms. The advantage of uncharged particles might be the longer coherence time. The required ability to store individual atoms and to control their external and internal degrees of freedom was realized in our group within the last years. We are able to store a desired number of neutral Cs atoms, to move them with sub-micrometer precision and to manipulate their internal quantum states. Also, the coherence time of internal states was measured [Kuhr03]. The next step towards quantum information processing is the interaction between two atoms. In this case the lack of Coulomb interaction requires additional effort to establish such interaction. In free space, neutral atoms interact considerably strongly only at very short distances. Our approach is to use an optical resonator in which the atom-atom interaction is mediated via the exchange of a photon.

The subject of this work is the preparation of suitable optical resonator which continues the work of Y. Miroshnychenko [Mir02]. In order to perform experiments with atoms in a cavity, the system must fulfill the condition of *strong coupling*, where the coherent interaction between the atom and the intracavity field dominates over the dissipation. The dissipation is due to the limited lifetime of photons in the cavity and atomic decay. Quantitative understanding of the interaction of an atom with photons within the cavity requires advanced theoretical treatment. By solving the master equation of a two level atom interacting with the single mode cavity in presence of dissipation I have calculated the spectrum of the system.

The experimental challenge is to achieve a strong atom-photon interaction while keeping the dissipation low. The interaction increases when the photons are confined to a smaller volume, whereas the photon lifetime in the cavity can be improved by increasing the reflectivity of the mirrors. Altogether, the resonator must have a microscopic mode volume and high mirror reflectivity.

In order to sort out mirrors with best reflectivity from our set we need a quick method of mirror characterization. For these means I have implemented a cavity ring-down setup which measures the lifetime of a photon in a cavity.

The precise control of interaction parameters requires the ability to tune the cavity resonance frequency and to keep it stable for the time of the experiment. Since the resonance frequency depends on cavity length changes on a picometer scale, an active feedback scheme is required to achieve the necessary stability. Our scheme is based on stabilization of the cavity to a laser and incorporates the Pound-Drever-Hall method. This scheme was completed, optimized and characterized.

Chapter 1

Theory

1.1 Optical resonators

An optical resonator is a “container” for light, it is able to store photons for a certain time within its volume.

1.1.1 Basic properties

An optical resonator basically consists of two opposing mirrors. First we consider a simple model, the so called Fabry Perot resonator of two plane mirrors, fig. 1.1. It describes most of the properties of real resonators.

The relevant parameters are the resonator length L and the mirror reflectivities R_1, R_2 and transmissions T_1, T_2 . For convenience we set $R = \sqrt{R_1 R_2}$, $T = \sqrt{T_1 T_2}$.

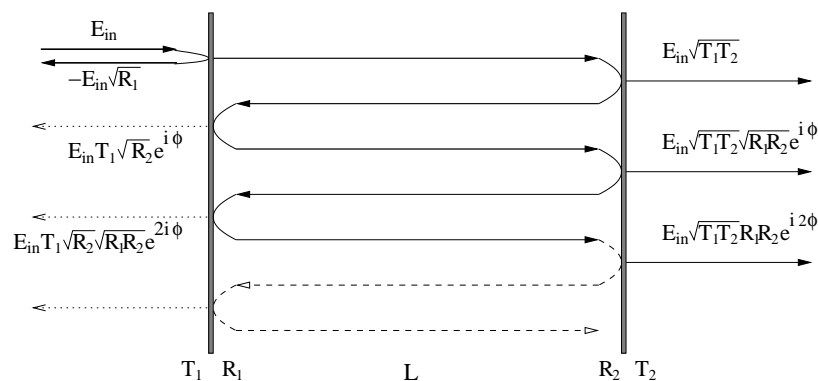


Figure 1.1: Fabry-Perot resonator. An incident electromagnetic wave leads to a series of partial reflections.

A laser beam of frequency ω and wave-vector $k = \frac{\omega}{c} = \frac{2\pi}{\lambda}$ incident on one mirror is partially transmitted and partially reflected. The transmitted part enters the resonator and is reflected forth and back many times. On each reflection a fraction escapes the resonator, see fig. 1.1. Since this process is coherent, the amplitudes of the reflections will interfere.

The transmitted field amplitude is the sum of all amplitudes after the second mirror:

$$E_t = E_{\text{in}}(T + TRe^{i\phi} + TR^2e^{i2\phi} + \dots) = E_{\text{in}} \frac{T}{1 - Re^{i\phi}},$$

where $\phi = 2Lk$ is the **round-trip phase** of the light wave in the resonator. Similarly, the reflected field is

$$E_r = E_{\text{in}}(-\sqrt{R_1} + T_1e^{i\phi}\sqrt{R_2} + T_1\sqrt{R_2}Re^{2i\phi} + \dots) = E_{\text{in}}(T_1 \frac{\sqrt{R_2}e^{i\phi}}{1 - Re^{i\phi}} - \sqrt{R_1}). \quad (1.1)$$

The transmitted intensity is proportional to the square of the field:

$$I_t \sim |E_t|^2 = E_{\text{in}}^2 \left| \frac{T}{1 - Re^{i\phi}} \right|^2 = E_{\text{in}}^2 \frac{T^2}{(1 - R)^2} \frac{1}{1 + \frac{4R}{(1-R)^2} \sin^2(\frac{\phi}{2})}. \quad (1.2)$$

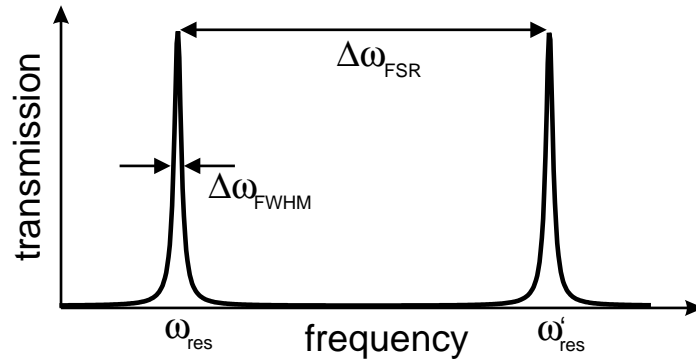


Figure 1.2: Transmission of an optical resonator.

Maximal transmission of $\frac{T^2}{(1-R)^2}$ occurs at the resonance frequencies ω_{res} when all reflections interfere constructively, i.e. the round trip phase is a multiple of 2π :

$$\frac{2L}{c}\omega = \phi \stackrel{!}{=} 2\pi \cdot q, \quad q = 1, 2, \dots$$

The resonance frequencies are then

$$\omega_{\text{res}} = 2\pi \frac{c}{2L} q =: \Delta\omega_{\text{FSR}} \cdot q, \quad q = 1, 2, \dots$$

The spectrum is periodic, with a period of $\Delta\omega_{\text{FSR}} := 2\pi \frac{c}{2L}$, called the **free spectral range**.

From eq. (1.2) we calculate the **linewidth** $\Delta\omega_{\text{FWHM}}$ of the resonances:

$$\Delta\omega_{\text{FWHM}} = \Delta\omega_{\text{FSR}} \frac{1-R}{\pi\sqrt{R}} =: \frac{\Delta\omega_{\text{FSR}}}{F}.$$

The factor

$$F := \frac{\pi\sqrt{R}}{1-R} = \frac{\Delta\omega_{\text{FSR}}}{\Delta\omega_{\text{FWHM}}} \quad (1.3)$$

is called the **finesse** of the resonator, and depends only on the mirror reflectivity.

The field in the resonator is a standing wave. We consider the case of resonance for a symmetric resonator: $R_1 = R_2 = R$, $T_1 = T_2 = T$. At an anti-node all forth and back reflections interfere constructively and give the resonant intra-cavity field strength

$$E_{\text{cavity}} = E_{\text{in}} \sqrt{T} (1 + \sqrt{R}) (1 + R + R^2 + \dots) = E_{\text{in}} \frac{\sqrt{T}(1 + \sqrt{R})}{1-R}.$$

For a high reflectivity without losses we have $R \approx 1$, $T = 1 - R$ and thus

$$E_{\text{cavity}} \approx E_{\text{in}} \frac{2}{\sqrt{1-R}}.$$

The resonant **intra-cavity intensity** in an anti-node is then

$$I_{\text{cavity}} = I_{\text{in}} \frac{4}{1-R} \approx 4 \frac{F}{\pi} I_{\text{in}}. \quad (1.4)$$

The cavity enhances the intensity by a factor $\frac{4}{\pi}F$. This is one reason for the usage of cavities in experiments with atoms. If one is able to obtain a high finesse, the interaction of atoms with a laser beam is enhanced by several orders of magnitude compared to interaction in free space. If an atom is not localized to an anti-node along the resonator axis (as will be the case in our setup) it will see an average intensity over one or several periods of the standing wave:

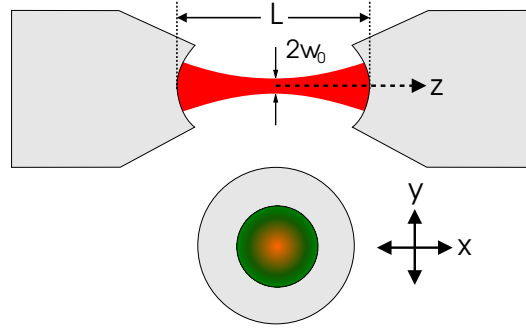
$$I_{\text{cavity}}^{(\text{mean})} = 2 \frac{F}{\pi} I_{\text{in}}.$$

1.1.2 Eigenmodes

Real resonators are typically built with spherically concave mirrors. Here, the field is confined in three dimensions to a mode of a finite volume.

We consider a symmetric resonator of two identical mirrors. The resonator is radially symmetric, has the length L and mirror curvature radius R_c . We call the resonator axis z and set $z = 0$ in the center, see fig. 1.3.

The field inside the resonator is the solution of Maxwell equations with boundary conditions (mirrors). The eigenmodes can be described in the paraxial approximation by standing wave Hermite-Gaussian modes (see e.g. [Sie86]):

Figure 1.3: Fundamental TEM₀₀ mode.

$$E_{m,n}(x,y,z,t) = E_0 X_m(x,z) Y_n(y,z) e^{-ik(z-\frac{L}{2})} e^{i(\omega t)} + c.c.$$

$$X_m(x,z) = \frac{1}{\sqrt{w(z)}} H_m\left(\sqrt{2}\frac{x}{w(z)}\right) \exp\left(-\frac{x^2}{w^2(z)} - i\frac{kx^2}{2R(z)} + i\frac{2m+1}{2}\psi(z)\right)$$

$$Y_n(y,z) = \frac{1}{\sqrt{w(z)}} H_n\left(\sqrt{2}\frac{y}{w(z)}\right) \exp\left(-\frac{y^2}{w^2(z)} - i\frac{ky^2}{2R(z)} + i\frac{2n+1}{2}\psi(z)\right)$$

with

$$w_0 : \text{mode waist}, \quad w(z) = w_0 \sqrt{1 + \left(\frac{z}{z_R}\right)^2} : \text{mode radius} \quad (1.5)$$

$$z_R = \frac{\pi}{\lambda} w_0^2 : \text{Rayleigh range}$$

$$R(z) = z + \frac{z_R^2}{z} : \text{wavefront curvature}$$

$$\psi(z) = \arctan\left(\frac{z}{z_R}\right) : \text{Guoy phase.}$$

Here $H_j(x)$, $j = 0, 1, 2, \dots$ are the corresponding Hermite polynomials of the order j . The solutions for different $m, n \in \mathbb{N}$ have different field distribution in radial direction and are called TEM _{m,n} transversal modes.

The boundary condition is, that on reflection the curvature radii of the wavefront and the mirror must be equal, i.e. $R(\frac{L}{2}) \stackrel{!}{=} R_c$. This determines the waist w_0 :

$$w_0^2 = \frac{\lambda}{\pi} \sqrt{\frac{L}{2} \left(R_c - \frac{L}{2}\right)}. \quad (1.6)$$

The most important mode is TEM₀₀ or fundamental mode:

$$E_{0,0}(x,y,z) = E_0 \frac{1}{w(z)} \exp\left(-\frac{r^2}{w^2(z)} - i\frac{kr^2}{2R(z)} + i\psi(z)\right) e^{-ik(z-\frac{L}{2})} + c.c. \quad (1.7)$$

with $r^2 := x^2 + y^2$. This corresponds to two counter-propagating Gaussian beams. We will work with this mode in the resonator since it has the most homogeneous radial intensity distribution without nodes.

Because of the Guoy phase the different transversal modes are non-degenerate. The round trip phase is

$$\begin{aligned} \phi_{n,m} &= 2Lk - 2(m+n+1)\left(\psi\left(\frac{L}{2}\right) - \psi\left(-\frac{L}{2}\right)\right) = \\ &= \frac{2\pi}{\Delta\omega_{\text{FSR}}}\omega - 2(m+n+1)\arccos\left(1 - \frac{L}{R_c}\right). \end{aligned}$$

The resonance condition is $\phi_{n,m} \stackrel{!}{=} 2\pi q$, $q = 1, 2, \dots$. We get

$$\omega_{n,m} = \Delta\omega_{\text{FSR}} \left(q + \frac{1}{\pi}(m+n+1)\arccos\left(1 - \frac{L}{R_c}\right) \right). \quad (1.8)$$

The resonance frequencies of transversal modes are equidistant. q is the longitudinal order, i.e. the number of antinodes in the resonator. The modes with equal $(m+n)$ are degenerate. The mode separation depends on the length of the resonator, we will use this relation later to measure the mirror distance of an assembled cavity.

In the experiment we often scan the mirror distance and not the laser frequency. A change of $\frac{\lambda}{2}$ in the distance corresponds to $\Delta\omega_{\text{FSR}}$. For $\Delta L < \frac{\lambda}{2} \ll L$ we have $\Delta\omega \propto \Delta L$ in very good approximation.

1.1.3 Quantization of the electromagnetic field

Up to now we dealt with classical electromagnetic fields in the resonator. In order to understand the quantum optical phenomena we need a treatment on a single photon level. The quantum field will be used to analyze the interaction of an atom with the cavity mode. The method for introducing photons is the canonical field quantization (see e.g. [Sho90], [Scu97]).

We consider monochromatic light of the frequency ω in the fundamental mode of the cavity. Suppose, it is linearly polarized, then there are only two mutually orthogonal components E and B of the field. The idea of the quantization is that for the standing wave fields in the resonator this problem has the structure of a harmonic oscillator. E plays the role of the ‘‘position’’ and B is the ‘‘momentum’’.

The quantum mechanical formalism expresses the field operators in terms of **creation** and **annihilation operators** \hat{a}^\dagger and \hat{a} :

$$\begin{aligned} \hat{E}(x,y,z) &= E_{00}(x,y,z)(\hat{a}^\dagger + \hat{a}), \\ \hat{B}(x,y,z) &= iB_{00}(x,y,z)(\hat{a}^\dagger - \hat{a}), \end{aligned}$$

where the spatial parts $E_{00}(x, y, z)$ and $B_{00}(x, y, z)$ are the same as in eq. (1.7).

The operators \hat{a}^\dagger , \hat{a} add and remove monochromatic, polarized photons in the resonator. The quantum mechanical expression for the energy is

$$\hat{H} = \hbar\omega(\hat{a}^\dagger\hat{a} + \frac{1}{2}).$$

The operator $\hat{a}^\dagger\hat{a}$ counts the number of photons, $\hbar\omega$ is the energy of a single photon. The energy eigenstates are photon number states

$$|0\rangle, |1\rangle, |2\rangle, \dots$$

In this picture the field in the resonator consists of photons which are reflected forth and back between the mirrors.

1.1.4 Photon lifetime

Since the reflectivity of the mirrors is limited, the photon will stay in the resonator only for a limited period of time. We can find it as follows:

The round trip time of the photon is $t_{\text{trip}} = \frac{2L}{c} = \frac{2\pi}{\Delta\omega_{\text{FSR}}}$. The intensity loss during half a round-trip (one reflection) is:

$$\begin{aligned} \frac{I(t) - I(t + \frac{1}{2}t_{\text{trip}})}{\frac{1}{2}t_{\text{trip}}} &= I(t) \frac{1-R}{\frac{\pi}{\Delta\omega_{\text{FSR}}}} = I(t) \cdot \sqrt{R} \frac{\Delta\omega_{\text{FSR}}}{F} = \\ &= I(t) \cdot \sqrt{R} \Delta\omega_{\text{FWHM}} \approx I(t) \cdot \Delta\omega_{\text{FWHM}}. \end{aligned}$$

Since the cavity is traversed at the velocity of light, t_{trip} is small and thus

$$\begin{aligned} \frac{I(t + \frac{1}{2}t_{\text{trip}}) - I(t)}{\frac{1}{2}t_{\text{trip}}} &\approx \frac{dI}{dt} = I(t) \cdot \Delta\omega_{\text{FWHM}} \\ \Rightarrow I(t) &= I_0 e^{-\Delta\omega_{\text{FWHM}}t} = I_0 e^{-\frac{t}{\tau}}. \end{aligned} \quad (1.9)$$

The intensity decays exponentially and

$$\tau := \frac{1}{\Delta\omega_{\text{FWHM}}} = \frac{F}{\Delta\omega_{\text{FSR}}} \quad (1.10)$$

is the **photon lifetime**.

One defines the **photon loss rate** as:

$$\kappa := \frac{1}{\tau}. \quad (1.11)$$

The mean number N of reflections in the cavity is given by:

$$N = 2 \frac{\tau}{t_{\text{trip}}} = 2 \frac{\Delta\omega_{\text{FSR}}}{2\pi\Delta\omega_{\text{FWHM}}} = \frac{F}{\pi}.$$

1.2 Atom-cavity interaction

With the basic properties of the resonator we can now analyze what happens with atoms in the cavity.

1.2.1 Atom-cavity coupling strength

To describe the atom in a way similar to the photon picture we use the second quantization formalism. We consider a two level atom with ground and excited states $|g\rangle, |e\rangle$ and introduce the operators $\hat{\sigma}^\dagger := |e\rangle\langle g|$ and $\hat{\sigma} := |g\rangle\langle e|$ which create and annihilate atomic excitation.

Suppose the atom is placed in an antinode of the standing wave, such that the spatial dependence of the interaction can be omitted. The dominating part is the interaction of the atomic dipole moment with the electric field component (dipole approximation).

The interaction Hamiltonian in the Heisenberg picture is

$$\hat{H}_{\text{int}} = \hat{d} \cdot \hat{E} = d(\hat{\sigma}^\dagger e^{i\omega_0 t} + \hat{\sigma} e^{-i\omega_0 t}) \cdot E(\hat{a}^\dagger e^{i\omega_c t} + \hat{a} e^{-i\omega_c t}),$$

where ω_0 is the atomic transition frequency, ω_c is the cavity photon frequency, \hat{a}^\dagger, \hat{a} create/annihilate cavity photons, d is the electrical dipole moment of the atom, and E is a constant which depends on the mode volume V (see [Scu97]):

$$E = \sqrt{\frac{\hbar\omega_c}{2\varepsilon_0 V}}$$

$$V = \frac{\pi}{4} w_0^2 L = \frac{\lambda}{4} L \sqrt{\frac{L}{2} \left(R_c - \frac{L}{2}\right)}.$$

The expression for the mode volume is valid for $L \ll z_R$.

In the rotating wave approximation ($\omega_0 - \omega_c \ll \omega_0 + \omega_c$) the Hamiltonian reduces to:

$$\hat{H}_{\text{int}} = dE(\hat{\sigma}^\dagger \hat{a} + \hat{\sigma} \hat{a}^\dagger) = \hbar g(\hat{\sigma}^\dagger \hat{a} + \hat{\sigma} \hat{a}^\dagger),$$

where

$$g := \frac{dE}{\hbar} = \sqrt{\frac{d^2 \omega}{2\hbar \varepsilon_0 V}} \quad (1.12)$$

is the **atom-cavity coupling rate**. This interaction Hamiltonian is also known as Jaynes-Cummings Hamiltonian [Jay63].

1.2.2 Jaynes-Cummings model

In the Jaynes-Cummings model we consider the interaction of a two level atom with a single mode optical cavity. The system shall be ideal, the atom can not decay spontaneously from the excited state to the ground state, and also photons do not escape the resonator.

The full Hamiltonian including the atomic and cavity energy is given by:

$$\hat{H} = \hbar\omega_0\hat{\sigma}^\dagger\hat{\sigma} + \hbar\omega_c(\hat{a}^\dagger\hat{a} + \frac{1}{2}) + \hbar g(\hat{\sigma}^\dagger\hat{a} + \hat{\sigma}\hat{a}^\dagger),$$

The atom can be excited by absorbing a cavity photon or go to the ground state giving its excitation to the cavity. Since

$$\hat{\sigma}^\dagger\hat{a} + \hat{\sigma}\hat{a}^\dagger = |e,n\rangle\langle g,n+1| + |g,n+1\rangle\langle e,n|,$$

the interaction couples the states $|g,n+1\rangle$ and $|e,n\rangle$ for each photon number n . In the submanifold of these two states we can write the Hamiltonian:

$$\hat{H}_n = \frac{\hbar}{2} \begin{pmatrix} (\omega_c - \omega_0) & 2\sqrt{n+1} \cdot g \\ 2\sqrt{n+1} \cdot g & -(\omega_c - \omega_0) \end{pmatrix},$$

which can be easily diagonalized giving the energy eigenvalues $\pm \frac{\hbar}{2} \sqrt{(\omega_c - \omega_0)^2 + 4(n+1)g^2}$.

The interaction lifts the degeneracy between the atom and the cavity. The eigenstates are split, see fig. 1.4, which is called **vacuum Rabi splitting**. In resonance, i.e. $\omega_c = \omega_0$, the splitting is $2\sqrt{n+1} \cdot \hbar g$. The coupled atom and cavity become one system with two resonances.

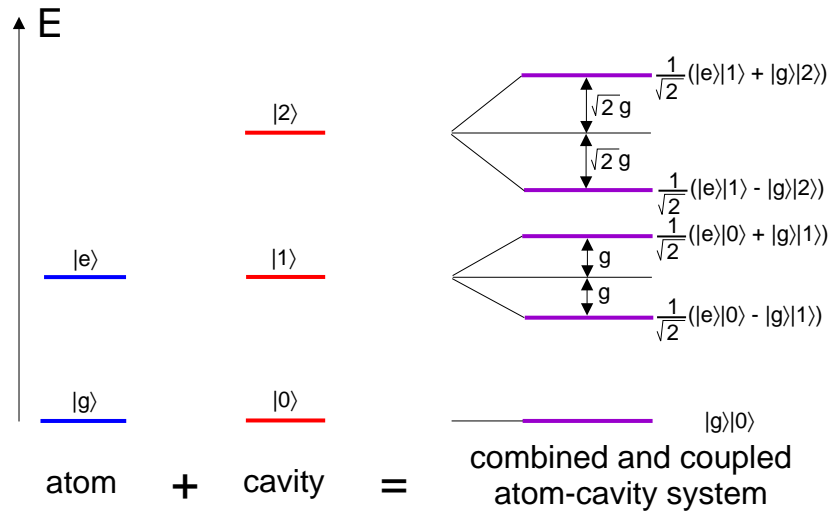


Figure 1.4: Eigenstates of the resonant atom-cavity system.

1.2.3 Dissipation and strong coupling

In the *real* atom-cavity system, the mirrors have a limited reflectivity and the atomic excited state has a finite lifetime. There are 3 important processes :

1. coherent atom-photon interaction at the rate g ,
2. incoherent photon leakage from the cavity at the rate κ ,
3. incoherent spontaneous decay of the atomic excited state at the rate Γ .

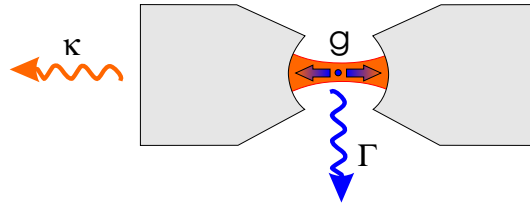


Figure 1.5: Parameters of atom-cavity system.

The two last processes lead to loss of coherence. In a cavity QED experiment one often wants to study or to use the coherent interaction with as little damping as possible. It means that the coherent evolution must be fast compared to the decoherence processes. One has to get into the regime of **strong coupling**:

$$g > \kappa, \Gamma.$$

This enables coherent energy exchange between atom and cavity within the lifetime of the atom-cavity system. For a large g the mode volume has to be small according to eq. (1.12). A low photon loss rate κ is achieved by a high reflectivity of the mirrors.

1.2.4 Density matrix approach

The dissipation does not only make the experiment difficult, its theoretical treatment also requires advanced tools. One has to consider the interaction of the system with the environment which leads to a thermal statistical equilibrium. This can be done in the density matrix formalism.

Our atom-cavity system is now coupled to the environment. The evolution of the whole system including the environment can be described by a Schrödinger equation. Since the exact quantum state of the environment is not known, one traces (takes the mean value) over environmental states and obtains the master equation [Car93]:

$$\frac{d}{dt}\hat{\rho} = \frac{1}{i\hbar}[\hat{H}, \hat{\rho}] + \frac{\kappa}{2}(2\hat{a}\hat{\rho}\hat{a}^\dagger - \hat{a}^\dagger\hat{a}\hat{\rho} - \hat{\rho}\hat{a}^\dagger\hat{a}) + \frac{\Gamma}{2}(2\hat{\sigma}\hat{\rho}\hat{\sigma}^\dagger - \hat{\sigma}^\dagger\hat{\sigma}\hat{\rho} - \hat{\rho}\hat{\sigma}^\dagger\hat{\sigma}). \quad (1.13)$$

Here, $\hat{\rho}$ is the density matrix for the atom-cavity system, κ are cavity losses, Γ is the decay rate of the atomic excited state. The first part of the master equation describes coherent evolution, the terms with κ and Γ are responsible for the dissipation processes which lead to decoherence. The Hamiltonian contains the atom and cavity energies, the atom-cavity interaction and coherent driving of the cavity by a laser field of frequency ω_l

$$\hat{H} = \hbar(\omega_0 - \omega_l)\hat{\sigma}^\dagger\hat{\sigma} + \hbar(\omega_c - \omega_l)\hat{a}^\dagger\hat{a} + \hbar g(\hat{\sigma}^\dagger\hat{a} + \hat{\sigma}\hat{a}^\dagger) + \hbar\varepsilon(\hat{a}^\dagger + \hat{a}).$$

In the presence of decoherence the master equation has a steady state $\frac{d}{dt}\hat{\rho} \stackrel{!}{=} 0$. This is a system of (infinitely many) homogeneous linear equations. Numerical tools for solving the master equation exist, e.g. [Tan02]. They provide the spectra of the system and expectation values of atom and cavity states by restricting the dimension of the Hilbert space to a computationally affordable value. The structure of the solution, however, remains hidden in this approach.

My goal was to find an analytical solution of the problem in a reasonable approximation. I have solved the master equation analytically in the case of a weak driving field. For details see Appendix A.

In case of resonance between atom and cavity, $\omega_c = \omega_0$, the result is

$$\rho_{11} = \frac{\varepsilon^2(\frac{\Gamma^2}{4} + \omega_l^2)}{\omega_l^4 + (\frac{1}{4}(\kappa^2 + \Gamma^2) - 2g^2)\omega_l^2 + (\frac{\kappa\Gamma}{4} + g^2)^2}$$

$$\rho_{22} = \frac{\varepsilon^2 g^2}{\omega_l^4 + (\frac{1}{4}(\kappa^2 + \Gamma^2) - 2g^2)\omega_l^2 + (\frac{\kappa\Gamma}{4} + g^2)^2},$$

where ρ_{11} is the probability of finding a photon in the cavity and ρ_{22} is the population of the excited state of the atom. The photon flux from the cavity is then $\kappa\rho_{11}$. The approximation requires that the driving laser field ε must be small, such that $\rho_{11}, \rho_{22} \ll 1$.

The figure 1.6 shows the Rabi splitting in this solution. The two curves are $\rho_{11}(\omega_l), \rho_{22}(\omega_l)$, i.e. the populations of cavity and atom excited states as functions of the driving laser detuning to atomic resonance. The first one is equivalent to the transmission spectrum of the cavity with an atom inside, when probed by a weak laser. The width of the lines is a sign of the presence of dissipation.

Analysis

To connect this result to the Jaynes-Cummings model, we determine the splitting of the peaks and the linewidth of the cavity transmission. For this purpose we rewrite the expression for ρ_{11} into two separate peaks:

$$\rho_{11}(\omega_l) = \frac{\varepsilon^2}{2\delta} \left(\frac{\alpha + \omega_l}{(\omega_l - \beta)^2 + \gamma^2} + \frac{\alpha - \omega_l}{(\omega_l + \beta)^2 + \gamma^2} \right),$$

where $\alpha, \beta, \gamma, \delta$ are expressions in terms of g, κ, Γ . The peaks are asymmetrically broadened but in the regime of strong coupling still well separated. The vacuum Rabi splitting can be found by determining the positions of the maxima. The approximate expression is

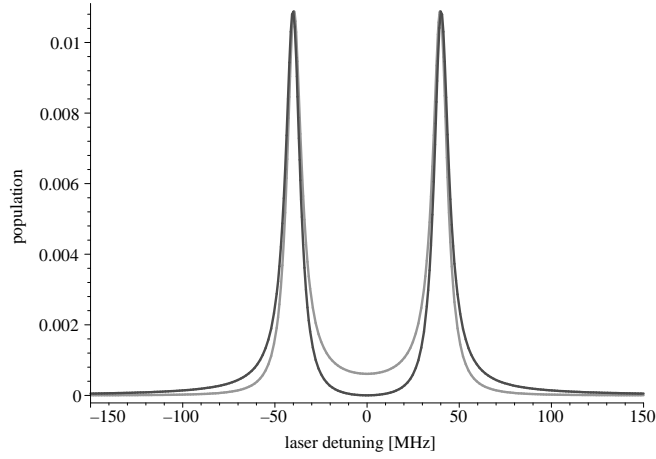


Figure 1.6: Rabi splitting in density matrix solution. Shown is the case of cavity resonant with the atom (centered at the origin). The parameters are $(g, \kappa, \Gamma) = 2\pi \cdot (40, 14, 5.2)$ MHz. The dark curve is the cavity population vs. laser detuning, the grey curve shows the atomic excitation.

$$\Delta_{\text{Rabi}} = 2\sqrt{g^2 + \frac{\kappa\Gamma}{4}},$$

which for strong coupling ($\kappa, \Gamma \ll g$) becomes $2g$ as in Jaynes-Cummings model.

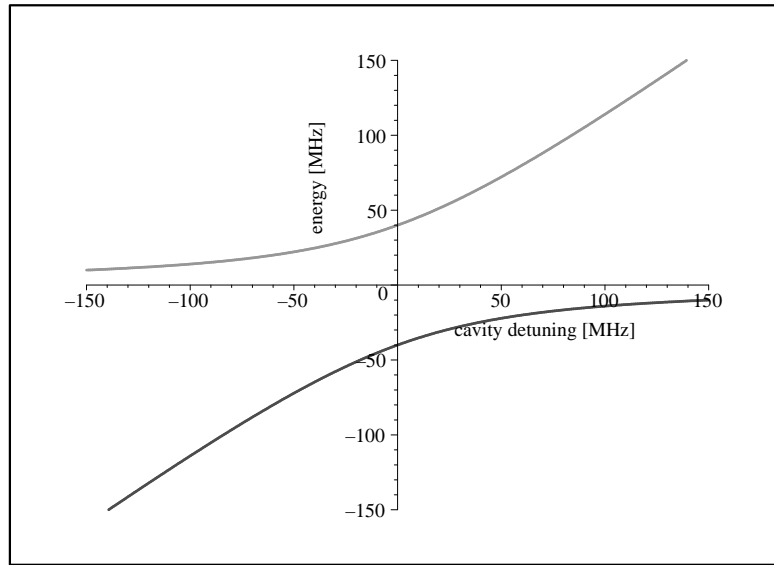
Because of the peak asymmetry, an effective linewidth is defined as the area under the peak divided by the peak height:

$$\Delta_{\text{FWHM}}^{(\text{eff})} := \frac{2 \text{ area}}{\pi \text{ height}}.$$

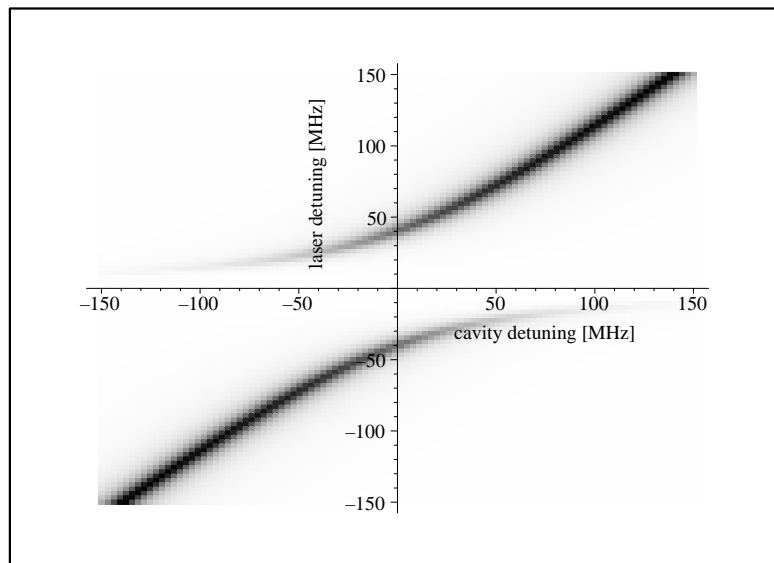
For a Lorentzian function this expression yields the FWHM linewidth. Using this definition we obtain the approximate expression:

$$\Delta_{\text{FWHM}}^{(\text{eff})} = \frac{\kappa + \Gamma}{2}.$$

Another important property is the dependence of energy eigenstates on the detuning of cavity with respect to atomic resonance. Figure 1.7 shows the eigenstates of the Jaynes-Cummings model (a) compared to the cavity spectra (b). The x axis is the cavity detuning from atomic resonance, the y axis is the energy (a), or detuning of the probe laser (b). One can see that the behavior of energy states is similar in both models.



(a)



(b)

Figure 1.7: (a) Energy levels of the Jaynes-Cummings model vs. cavity detuning. (b) Cavity photon number of density matrix solution vs. cavity- and probe laser detuning. The white area corresponds to 0 photons, black area to 0.02 photons in the cavity for $\epsilon = 1$. The atomic resonance is centered at the origin. The parameters are $(g, \kappa, \Gamma) = 2\pi \cdot (40, 14, 5.2)$ MHz.

1.2.5 Interaction between two atoms

Two atoms which simultaneously couple to the same cavity mode become mutually coupled and can exchange energy (information) via a cavity photon.

Suppose the atoms are at different positions within the mode and thus have in general different couplings g_1, g_2 . The interaction Hamiltonian with the cavity is the sum of two single-atom interactions:

$$\hat{H}_{\text{int}} = \hbar g_1 (\hat{\sigma}_1^\dagger \hat{a} + \hat{\sigma}_1 \hat{a}^\dagger) + \hbar g_2 (\hat{\sigma}_2^\dagger \hat{a} + \hat{\sigma}_2 \hat{a}^\dagger).$$

If the cavity is tuned far from the atomic resonance, the exchange of excitation between atom and cavity becomes negligible. Two atoms can still exchange their excitation via the cavity. The effective second order interaction Hamiltonian is

$$\hat{H}_{\text{int}}^{(2)} = \hbar \frac{g_1 g_2}{(\omega_c - \omega_0)} (\hat{\sigma}_1^\dagger \hat{\sigma}_2 + \hat{\sigma}_1 \hat{\sigma}_2^\dagger).$$

This is a two-photon process, where one atom emits a (virtual) photon into the cavity mode and the other one absorbs it. Both processes happen simultaneously, the excited state population remains small and can be *adiabatically eliminated*. One gets a *cavity induced* atom-atom interaction.

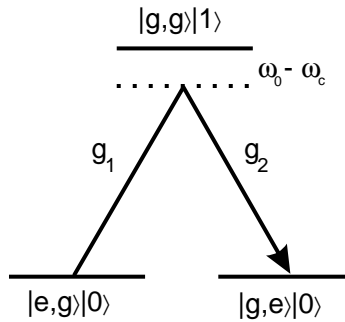


Figure 1.8: Cavity which is detuned far from the atomic resonance couples two atoms via a virtual cavity excitation.

The interaction described above has a long range because the radiation is concentrated into a single mode. For close distances between the atoms it is also possible to observe cavity amplified dipole-dipole or van der Waals interaction (see for example [Osn01]).

This scheme is only one possibility for coupling of two atoms via the cavity. There exist different schemes which propose to use the cavity for conditional quantum logic and entanglement (e.g. [Yi02]). The goal of future work in our group will be to implement one of those schemes to entangle two atoms.

Chapter 2

Cavity setup

The task to achieve strong coupling represents an experimental challenge. In order to perform experiments with Cs atoms, where the excited state decay rate is $\Gamma = 2\pi \cdot 5.2\text{MHz}$, to achieve $g > \Gamma$ we need a mode volume $V < 7.8 \cdot 10^5 (\mu\text{m})^3$. To minimize the photon loss rate κ , the mirror reflectivity should be as high as possible. We have set up a resonator with the goal to fulfill these requirements. At the same time, the resonator has to be combined with our setup which delivers single cold Cs atoms. A suitable mechanical mounting system was built up and tested together with the cavity.

2.1 Resonator assembly

The first resonator was built for testing purposes by Y. Miroshnychenko in [Mir02]. Our next task was to set up a new resonator which can be integrated in our setup.

2.1.1 High reflectivity mirrors

The mirrors are manufactured by the company Research Electro Optics, Boulder, USA. The high reflectivity is achieved by a stack of several ten dielectric $\lambda/4$ layers. The specified reflectivity of the mirrors is $R = 99,997\%$ for the wavelength of the Cs D_2 line (852 nm), corresponding to a finesse of 104000. The spherical concave surface has a diameter of 1 mm and radius of curvature of $R_c = 10\text{mm}$, see fig. 2.1. The special conical shape of the substrate is needed because of the limited space in our setup as shown in sec. 2.3.4.

We have ordered a set of 30 mirrors. In [Mir02] two resonators were built showing a finesse of 77000 and 94000, both below specification. This shows that a careful inspection and characterization of the mirrors is needed before assembling a resonator.

At this point the tools for such a characterization were quite limited. At the beginning we inspected the mirrors visually with a 100x microscope. It provides light-field and dark-field observation. Using this microscope we have seen spots of different sizes on almost all mirrors. Those were ranging from macroscopic dust or glass particles down sub micrometer surface defects. By illuminating the surface from the side we were also able to see thin scratches on many

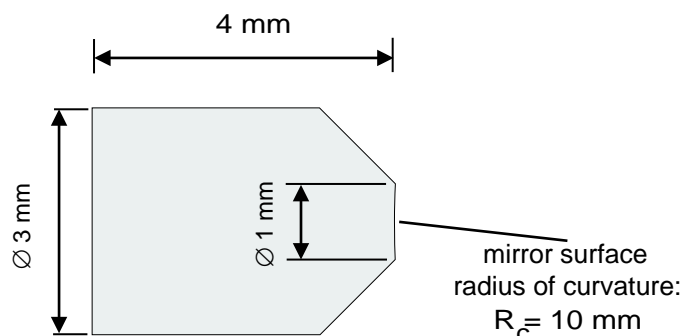


Figure 2.1: High reflectivity mirror, manufactured by the REO company.

mirrors. Then we used another microscope with 500x magnification which provides light-field, dark-field and better resolution. The closer look revealed more scratches and even more spots of sub-micrometer size, one example is shown in fig. 2.2. All visible defects reduce the finesse by scattering or absorbing light.

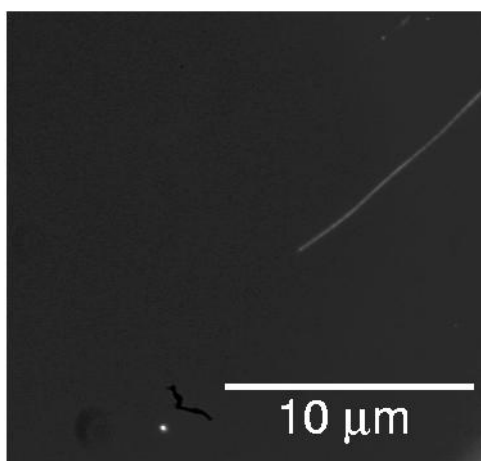


Figure 2.2: Microscope picture of the mirror surface, 500x magnification, dark-field observation. One sees a thin scratch, one clearly visible spot on the lower left and 3 smaller spots on the upper right. The dark objects in the lower part are defects of the camera.

In order to achieve the best finesse, we looked for mirrors which were free from defects in the center part of the mirror surface (~ 0.25 mm radius). Since the TEM_{00} mode will have a radius of about $15 \mu\text{m}$ this should guarantee that the defects do not limit the finesse. Since all mirrors have at least several spots in the center part, we chose mirrors without scratches in this region. Scratches are permanent, while spots can be small dust or glass particles, thus it might be possible to remove them. Due to the small mirror size and sensitivity of the mirror coating, special care has to be taken when trying to clean the surface.

We investigated the following methods for removing spots:

- **OptiClean:** a droplet of special polymer (manufactured by Merchan Tek Inc., San Diego, USA) is placed on the surface and covered with a piece of cleaning tissue. The polymer flows over the surface as a homogeneous layer and embeds the particles. After the drying (15-20 min) the tissue is easily removed together with the polymer. Bigger particles can be removed this way. Only a part of smaller particles is removed, several repetitions of the procedure are needed and it does not guarantee the removal of all particles. In rare cases the polymer can stick to the side of the mirror if too much was used, this residue has then to be removed with acetone. In general, using the polymer is fast and safe, since there is almost no risk of damaging the surface.
- **mechanical cleaning:** a piece of lens cleaning tissue is folded, wet in acetone and swept with a tweezer from the center to the border of the mirror. This method is difficult and dangerous since it is possible to produce additional scratches by dragging a piece of glass over the surface. We tried this method but decided not to use it because it had nearly no effect on smaller spots.
- **bathing in acetone or methanol:** the mirror is placed into warm acetone or methanol of ultra high purity. After about 5 minutes the mirror is taken out holding the surface vertical such that no liquid drop can stay on the surface. If some liquid would dry out on the surface, it would leave the dissolved dirt behind. This method is able to remove some of the spots, even small ones, but it can also add spots on some cases. It also removes the residue of the OptiClean polymer which could stick to the side of the mirror and cause problems with the ultra high vacuum needed in the experiment.
- **ultrasonic bath:** the mirror is placed into a small vessel filled with pure acetone and put into an ultrasonic bath for about 5 min. This device is filled with water and produces ultrasonic vibrations of the liquid which remove particles from the surface. However particles can produce scratches. Small spots are not removed.

After considering all methods we decided to clean selected mirrors by applying OptiClean several times and then doing both an acetone and a methanol bath. The surfaces were inspected after cleaning with the 500x microscope and the procedure was repeated when necessary. By these means we were able to find a mirror pair with no visible scratches and almost no spots in the center region of the surface.

2.1.2 Assembly

Piezo elements

For precise control of the resonator length the mirrors are glued onto piezo elements. We use shear piezos (PI Ceramic, 6x6x1 mm), which perform a shear movement of ± 300 nm when a voltage of ± 500 V is applied. This is enough to scan over a free spectral range of $\frac{\lambda}{2} = 426$ nm even when only one piezo is used.

Holder

The holder for the mirrors is designed for precise positioning of the cavity in our setup. It is described in all detail in sec. 2.3.4.

The procedure of assembly is almost the same as described in the diploma thesis [Mir02]. First, the piezo elements are glued onto the holder. The holder also provides electric ground contact. Before gluing, the mirrors are fixed to the piezo surfaces with a positioning tool which aligns them coaxially in a V-groove, see fig. 2.3. This ensures that the mode is well centered to the axis of both mirrors.

The next step is gluing of the mirrors to the piezo elements. The previous method was to put a glue droplet under the mirror, where it distributes as a thin layer. The problem of this approach is that the glued surface is big. When the glue cures it can contract introducing mechanical tension to the mirror substrate. This tension leads to a birefringence and should be avoided. The general rule is to reduce the contact area of the glue, presumably to only one or two points. The idea is to put the glue not directly between the mirror and the piezo but rather to use an additional glass cylinder (glass fiber) of few hundred micrometer diameter lying parallel to the mirror side. It is glued with one side to the piezo and with the other side to the mirror (see figure). Using the cylinder has also an additional advantage that it might be possible to remove a glued mirror. When glued directly, the removal destroys the mirror and the piezo, because of the large contact area with the glue. Figure 2.4 shows the assembled cavity on the holder.

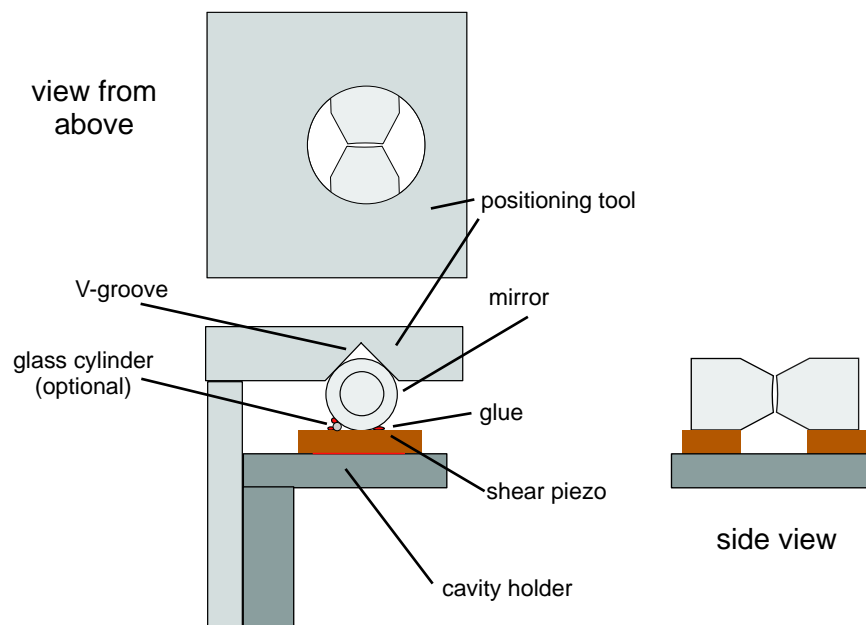


Figure 2.3: Assembly of the cavity.

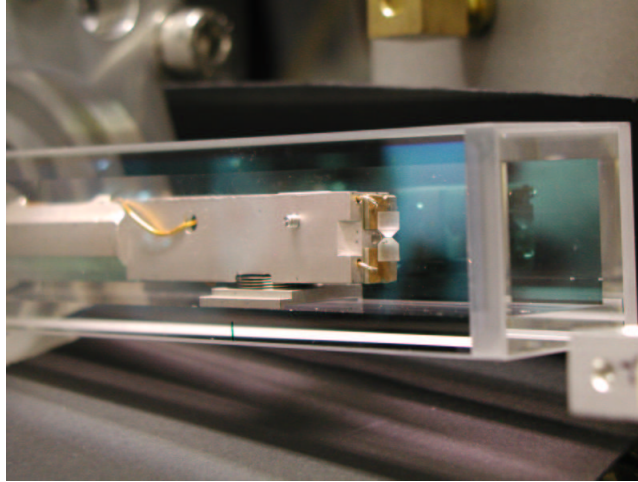


Figure 2.4: Assembled cavity in the glass cell of the test vacuum setup.

2.2 Characterization of the cavity

The most important parameters of the resonator are its length and the linewidth. Knowing them one can calculate the values of g and κ which are important for future cavity QED experiments.

Cavity test setup

For characterization and testing purposes the cavity was placed inside a vacuum chamber which is geometrically identical to the vacuum chamber of the main experiment. By doing so we are able to test the interplay of the cavity holder with the chamber geometry. This is important for later integration of the resonator into the main setup, for details see section 2.3.4. The optical part of the setup is shown in fig. 2.5.

There are two lasers in the setup, the probe laser (852 nm) and the lock laser (836 nm). The probe laser is resonant with the Cs atom, the second is used for cavity stabilization as described in the next chapter. Both lasers are delivered by the same fiber in orthogonal polarizations and are thus perfectly overlapped which reduces the amount of work for coupling them into the cavity.

The laser beams pass a specially designed mode matching telescope (see [Mir02], p. 23) which tailors their waist to match the fundamental TEM_{00} cavity mode. The geometrical coupling into the cavity mode is done with two mirrors. The transmitted light is imaged onto a CCD camera, which enables us to distinguish transversal modes. The transmitted power is measured with a photo-multiplier (Hamamatsu H7712-03). In order to reduce the straylight, a $200\ \mu\text{m}$ pinhole is placed in front of the detector.

The reflected beam passes back through the telescope, is coupled out with an unpolarizing beam-splitter and is focussed onto a fast photodiode (Newport amplified silicon PIN, 818-BB-21A). Its signal is used for the Pound-Drever-Hall stabilization of the QED cavity.

The voltage for the piezo elements is a triangle scan with variable amplitude and offset, which

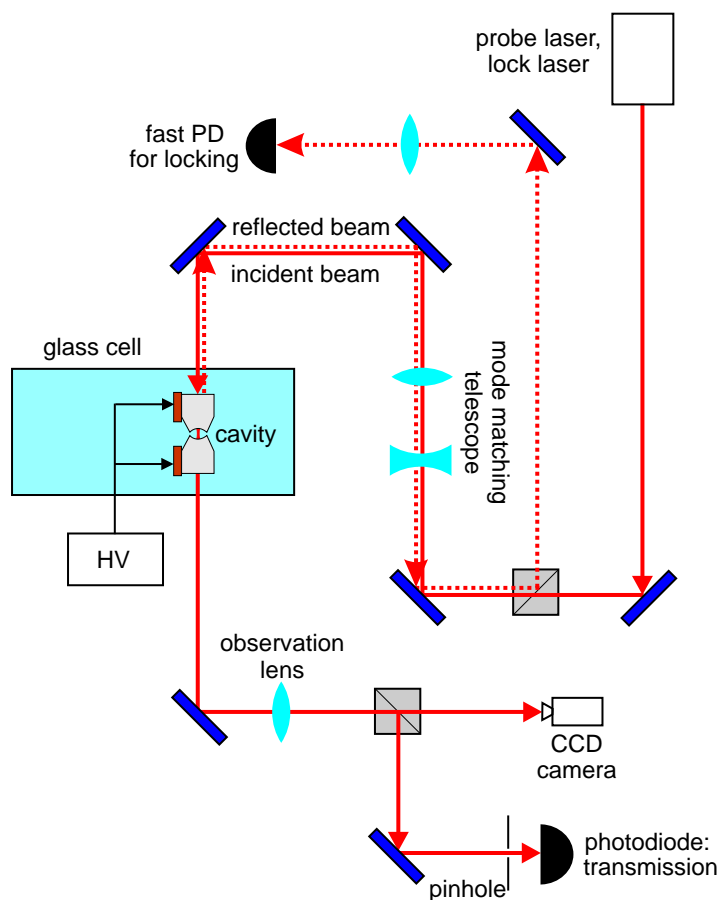


Figure 2.5: Optical setup for characterization and stabilization of the cavity.

is amplified to the necessary high voltage ($\pm 400\text{ V}$) by a low noise amplifier (FLC Electronics, A800-40).

Mode matching

In order to achieve the coupling of the laser into the fundamental cavity mode it is necessary to adjust the focus and the geometrical position of the beam to match the mode. The piezos are scanned at an amplitude of about 100 V at 10 Hz . The incidence position and angle of the beam are changed with a mirror and one tries to see some transmission on the camera. The laser can be approximately adjusted to the center of the cavity mirror. If no transmission is seen, the voltage offset for the piezo is changed and the procedure is repeated. If at least one higher transversal mode is visible, one can look in its vicinity for the neighboring lower mode by slightly changing the coupling angle. For identifying the individual transversal modes, the scan amplitude is reduced. By these means one moves down to the fundamental mode which is

then optimized with both mirrors. A coupling efficiency of 50% in the fundamental mode can be usually reached without additional effort. For a better coupling one can also adjust the telescope with and change its focus.

2.2.1 Voltage-travel relation of piezo elements

For precise control of the cavity resonance frequency one has to know precisely how the piezo elements change the resonator length with applied voltage. Their voltage-travel correspondence is in general nonlinear, given by the properties of the piezo material. As we know from eq. (1.8) the transversal modes of the resonator are equidistant and thus define a frequency scale. Therefore, we can measure the voltages corresponding to resonance of different transversal modes.

In order to get some intensity into the higher transversal modes, the coupling of the laser into the cavity was slightly misaligned. The piezo voltage was scanned slowly (1 Hz) over the maximal range (± 400 V) and the transmission peaks were recorded.

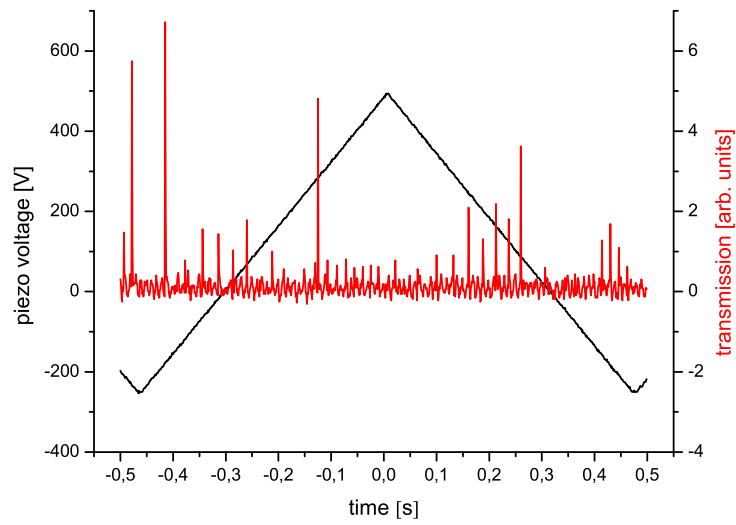
The transmission curve is shown in the figure 2.6, (a). It shows two free spectral ranges of the resonator. One can identify a large number of clearly visible transversal modes and assign them corresponding frequencies (transversal mode numbers). Due to the large scan range, the time during which the intensity of each mode is recorded is small, resulting in strong variations of the peak height.

The resulting response curve is shown in 2.6, (b). The displacement is slightly non-linear and depends quadratically on the voltage within this scan range. Additionally it has a hysteresis feature. Another important parameter is the voltage distance of two neighboring transversal modes for a small scan range (i.e. of the order of the mode separation itself). This distance was measured to be constant, its slope is shown in the curve. This is an important result, since the voltage-frequency relation is then linear and constant for small scan ranges used in the experiment or for stabilization.

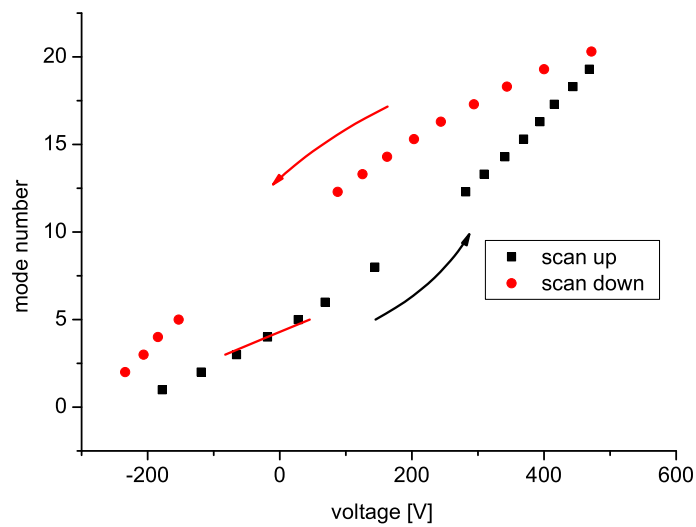
2.2.2 Resonator length

The control of the mirror distance during the assembly process is not very precise. The final distance is only known after the assembly is finished. It can, however, be deduced with high precision from the free spectral range or the frequency distance between transversal modes. The latter alternative is easier to measure since the transversal mode distance is small and thus still in the linear range of the piezo response. One problem is that the correspondence between the voltage scan and the frequency is unknown at this point. To get the absolute scale of frequency the laser beam is modulated by an AOM which produces a sideband at a defined distance from the main line, see fig. 2.7.

The procedure of measuring the distance between transversal modes is the following: both piezo elements are scanned in parallel at about 50 Hz, the scan amplitude is adjusted to be just above the spacing between neighboring modes. Then the mode distance is measured, together with the AOM sideband distance. Setting both values in relation one gets the result in frequency units. We measured the following value:



(a)



(b)

Figure 2.6: Measurement of the voltage-travel relation of the piezo elements. Figure (a) shows the transmission of transversal modes vs. mirror scan, figure (b) shows the response curve. The y-axis in (b) is proportional to the resonator length changes. For a small scan range between two neighboring modes one obtains a different response, which is also shown.

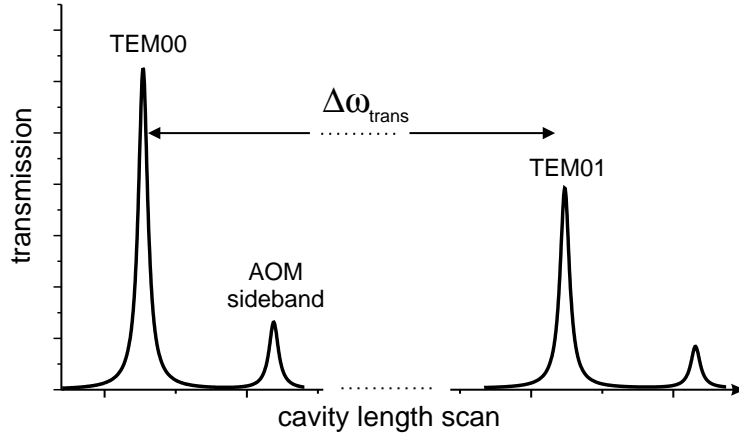


Figure 2.7: Measurement of the transversal mode distance (schematic). One sees the transmission of two neighboring transversal modes and the AOM sidebands.

$$\Delta\omega_{\text{trans}} = 2\pi \cdot 70.38 \text{ GHz.}$$

The error of this measurement is due to the limited resolution of the oscilloscope. It is of the order of 1 – 2%. A possible systematic error might be caused by the non-linearity of the piezo elements at the small scan range. This effect could not be measured, since there are no transmission lines between the neighboring transversal modes.

In order to calculate the cavity length L we use eq. (1.8) to get

$$\Delta\omega_{\text{trans}} = \frac{1}{\pi} \Delta\omega_{\text{FSR}} \arccos\left(1 - \frac{L}{R_c}\right) = \frac{c}{L} \arccos\left(1 - \frac{L}{R_c}\right).$$

This transcendental equation is solved numerically for L . The resulting cavity length is:

$$L = 92.2 \mu\text{m},$$

and the free spectral range is $\Delta\omega_{\text{FSR}} = 2\pi \cdot 1.63 \text{ THz}$.

The obtained value L is the *effective* cavity length. Since the mirror surface is a stack of dielectric layers, the light penetrates about $2 \mu\text{m}$ into the mirror, thus the physical mirror distance is slightly shorter.

2.2.3 Cavity linewidth and finesse

In order to obtain the photon loss rate κ and finesse F , we have to determine the spectral linewidth of the cavity. The cavity is scanned over the resonance of the TEM_{00} mode and the AOM sideband, see fig. 2.8. Similar to the previous measurement, the FWHM linewidth is compared to the distance of the AOM sideband. Knowing the AOM frequency, we directly get the linewidth.

The main difficulty of this measurement is the required stability of the resonator. All kinds of mechanical (acoustical) and electrical noise make the line move, fluctuate or change its shape.

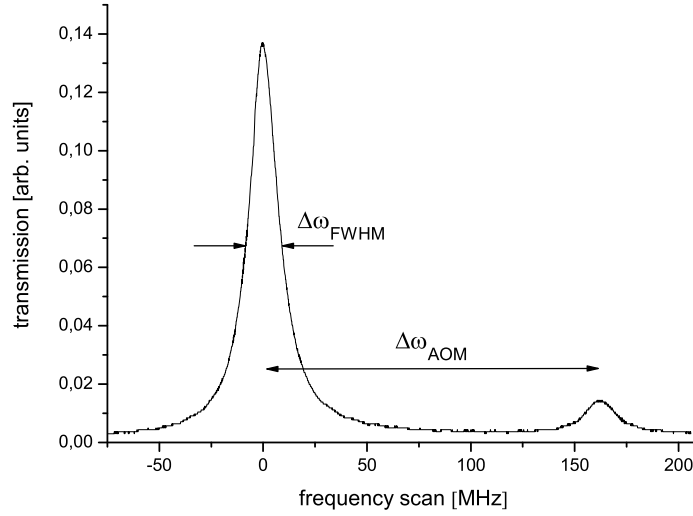


Figure 2.8: Cavity transmission showing the TEM_{00} line and its AOM sideband, averaged over 64 measurements.

Parts of the equipment, especially those which produce vibrations (e.g. vacuum pumps), have to be switched off.

We obtained the following values:

$$\kappa = \Delta\omega_{\text{FWHM}} = 2\pi \cdot 13.77 \text{ MHz},$$

$$F = \frac{\Delta\omega_{\text{FSR}}}{\Delta\omega_{\text{FWHM}}} = 118000.$$

The errors produced by the reading of the instrument are again 1 – 2%. The environmental noise, however, has a substantial impact on the linewidth. Performing this measurement in a somewhat noisier situation we obtained a larger linewidth of about 16 MHz.

The finesse is just above the specification of the manufacturer ($F_{\text{spec}} = 104000$) and is higher than the finesse achieved by the previous resonators ($F = 77000, 94000, 66000$). The shift of the resonance frequency of $\Delta\omega_{\text{FSR}}$ corresponds to a resonator length change of only $\frac{\lambda}{2} \cdot \frac{1}{F} \approx 3.6 \text{ pm}$, thus the length stability becomes an important issue.

2.2.4 Resulting parameters

Knowing the mirror distance of $L = 92 \mu\text{m}$ we can calculate the waist w_0 and the coupling parameter g .

According to eq. (1.6) : $w_0^2 = \frac{\lambda}{\pi} \sqrt{\frac{L}{2} (R_c - \frac{L}{2})}$. For $\lambda = 852 \text{ nm}$, $L = 92 \mu\text{m}$, $R_c = 10 \text{ mm}$ we get

$$w_0 = 13.5 \mu\text{m}.$$

The mode volume is $V = \frac{\pi}{4}w_0^2L$, for our parameters we get

$$V = 1.3 \cdot 10^4 (\mu\text{m})^3.$$

Finally we calculate the coupling parameter according to eq. (1.12):

$$g = \sqrt{\frac{d^2\omega}{2\hbar\epsilon_0V}}$$

using the values (see [Ste98]):

$d = 2.698 \cdot 10^{-29}$ Cm, $\omega = 2\pi \cdot 351.7$ THz we obtain

$$g = 2\pi \cdot 40.3 \text{ MHz}.$$

Altogether we have:

$$(g, \kappa, \Gamma) = 2\pi \cdot (40.3, 13.8, 5.2) \text{ MHz},$$

i.e.

$$\frac{g^2}{\kappa\Gamma} = 22.6.$$

which indicates that we should be able to achieve the strong coupling regime.

2.3 Single-atoms setup

Our main experimental setup allows us to deterministically deliver single cold Cs atoms to a defined position [Kuhr01]. Furthermore it is capable of preparation, coherent manipulation and measurement of the atomic hyperfine states, see [Kuhr03].

2.3.1 Single-atom MOT

Our source of single cold Cs atoms is a magneto-optical trap (MOT). It consists of three pairs of counter-propagating red detuned laser beams which constitute a so called optical molasses. The atoms from the dilute background Cs gas are Doppler cooled to a temperature of about $100 \mu\text{K}$. A high-gradient magnetic quadrupole field creates position dependent Zeeman splitting of the atomic hyperfine sub-levels. Together with the circular polarization of the beams this gives the position dependent restoring force needed for trapping. Details of the MOT are described in [Kuhr03]. The fluorescence light of the atoms in the trap is monitored by an avalanche photodiode. This enables us to count the exact number of atoms.

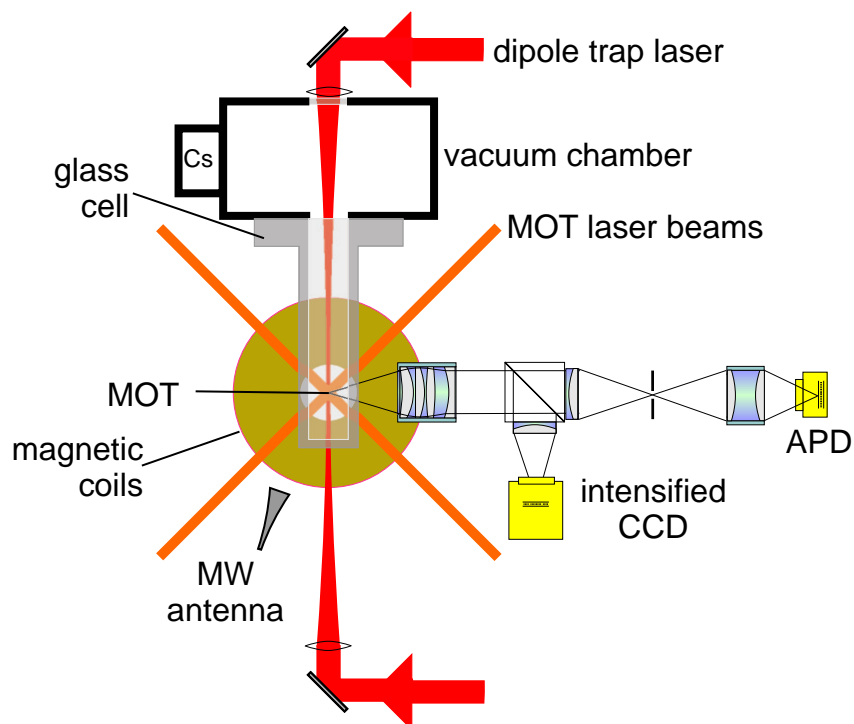


Figure 2.9: Experimental setup of our main experiment for the manipulation of single Cs atoms.

2.3.2 Optical conveyor belt

In order to control the position of the atoms, a second trap was set up. It is a far red-detuned dipole trap where atoms are attracted to regions of high laser intensity. It consists of two counter-propagating Gaussian beams of Nd:YAG laser (1064 nm, 4 W) which create a standing wave interference pattern with periodical potential wells of 532 nm separation. The dipole trap is overlapped with the MOT and the atoms can be efficiently transferred between the two traps. Thus, we can load the dipole trap with a desired number of atoms, from one to several ten. By changing the frequencies of the beams by means of two AOMs, the interference pattern is set into motion and carries the atoms. This optical “conveyor belt” is able to transport atoms over macroscopic distances (up to 10 mm) with sub-micrometer precision. Details about the conveyor belt can be found in [Sch01].

The atoms in the dipole trap can be observed spatially resolved by means of an intensified CCD camera. It observes the atoms via diffraction limited imaging optics enabling us to resolve atoms which are separated by more than $2\mu\text{m}$. With this tool it becomes possible to determine the position of an atom on the camera picture and to program the transport parameters such that it is moved to a defined position. This realizes an absolute position control which is one current work topic in our group.

2.3.3 Manipulation and measurement of internal states

The Cs atom has two hyperfine ground levels, $6S_{1/2} F = 3$ and $6S_{1/2} F = 4$, which can serve as a storage of quantum information (see fig. 2.10). The atoms can be initially prepared in either state in the MOT and then loaded into the dipole trap. For cavity QED experiments one must also coherently manipulate atomic hyperfine states. This is performed with microwaves at the hyperfine splitting frequency of 9.2 GHz. By applying resonant microwave pulses we can observe transitions between the ground states, also coherent superpositions of the states can be obtained this way. Another technique which we use are adiabatic passages, where a microwave frequency sweep efficiently transfers atoms from one state to the other. Alternatively we can also use optical Raman transitions (see [Dot02]).

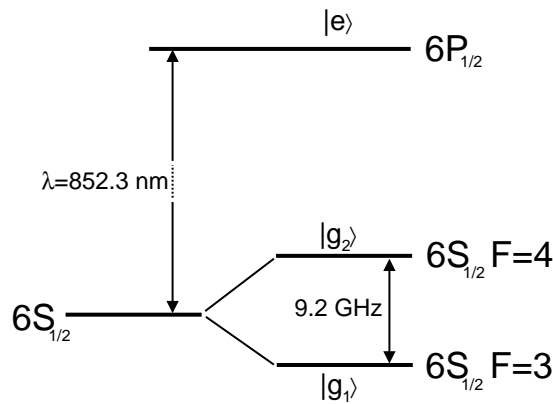


Figure 2.10: Cs atom as a three-level system. Shown are two long-lived hyperfine states and the excited state of the D_2 line. Hyperfine splitting of the $P_{1/2}$ state is omitted.

The measurement of the hyperfine state is performed by applying a laser which is resonant with the transition of one of the ground states to an excited level, removing the atoms in this state from the dipole trap. Details about microwave manipulation of the states and coherence properties of the atoms in the dipole trap can be found in [Kuhr03].

The manipulation techniques described above affect all atoms simultaneously. Current work in our group aims towards individual addressing of atoms in the dipole trap. With the help of microwave adiabatic passages in a magnetic field gradient it is possible to change the internal state of an atom on a defined position without affecting atoms on other positions. Using these methods we will prepare several atoms in different states. Their interaction within the cavity can then realize quantum logical operations.

2.3.4 Integration of the cavity into current setup

The goal is to combine our setup with the cavity such that the atoms can be transported from the source (MOT) into the interaction zone within the resonator by the optical conveyor belt. In order to transport the atoms into the cavity one has to align the conveyor belt laser from the side through the slit between the mirrors through the cavity mode. By properly adjusting the transport parameters, the atoms will be moved into the center of the mode which has a radius of $14\ \mu\text{m}$.

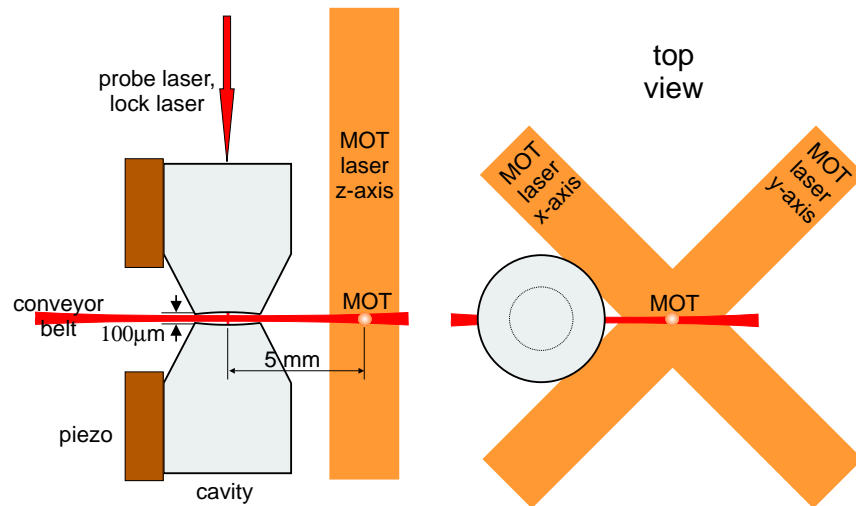


Figure 2.11: Planned setup geometry. The atoms will be transported over the distance of $5\ \text{mm}$ from the MOT into the cavity mode through the slit between the mirrors. The conical mirror shape leaves more space for the x-y MOT laser.

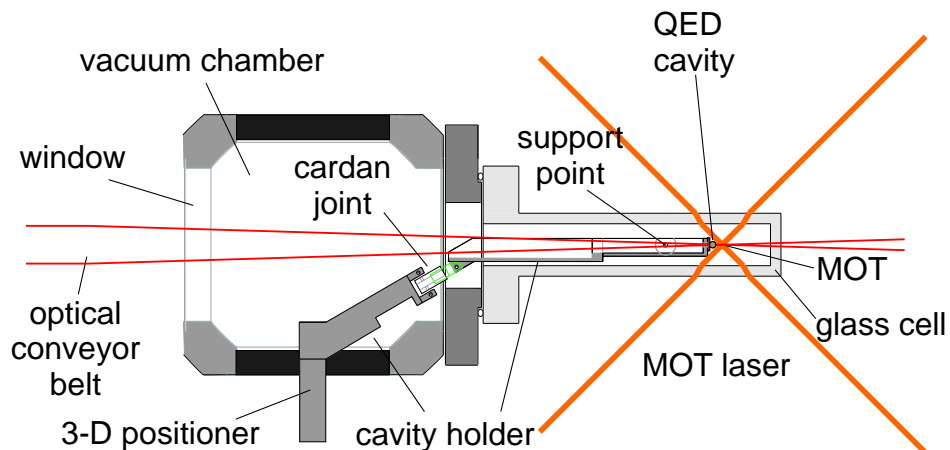


Figure 2.12: Top view of the chamber.

The integration shall follow the tactics of minimal invasion, i.e. the cavity has to be added into the setup without changing or disturbing the other parts. We aim a distance of 5 mm between the MOT center and the cavity center. The transportation has an efficiency over 80% for this distance and the conically shaped mirrors will not block the MOT lasers, see fig. 2.11.

The position of the MOT within the setup is fixed by the magnetic field zero and can not be changed. The position and direction of the optical conveyor belt also can not be changed without much effort. Thus the cavity has to be placed in the glass cell leaving the ability to change its position with high precision.

For these means the cavity is assembled on a specially designed holder. Its task is to transfer the movement of a precision 3D motional vacuum feed-through to the cavity. This positioning unit is controlled from outside the vacuum chamber giving the possibility to adjust the cavity position. The geometry is shown in fig. 2.12. The handling of the cavity with the holder is relatively tricky because of limited space in the vacuum chamber and the glass cell. Still, this is the only possibility to integrate the resonator without rebuilding the whole experiment. Figure 2.4 shows the cavity in the glass cell.

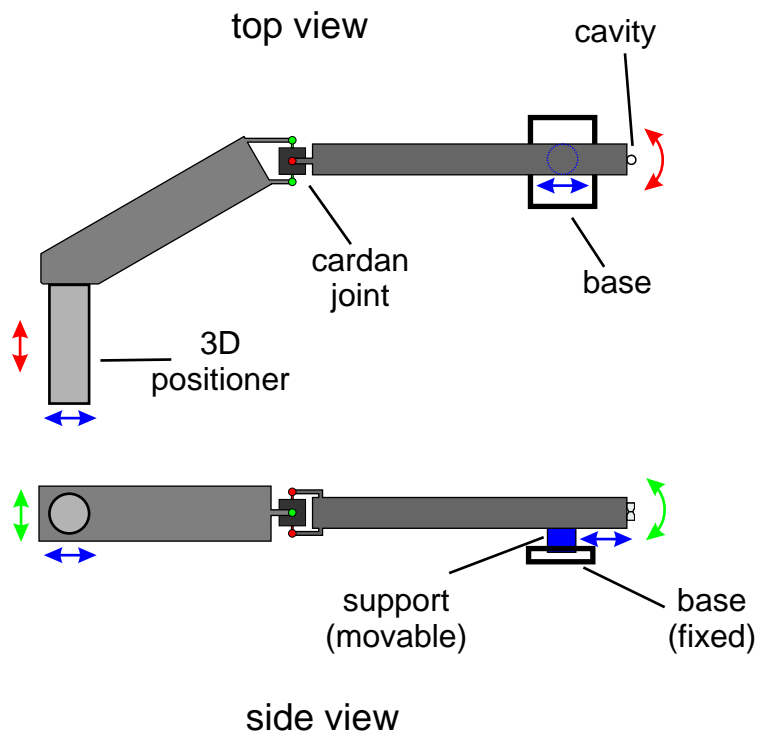


Figure 2.13: Kinematics of the cavity holder.

The holder consists of two parts which are connected by a cardan joint (see fig. 2.13). The part which holds the cavity rests on a support in the glass cell, the other part is attached to the 3D positioner. The support has the possibility to move along the base which is fixed in the glass cell. The 2 axes of movement of the positioner which are orthogonal to the cell axis are translated

around the support point by 1:5. The movement along the axis together with the support is translated 1:1.

The specified precision of the 3D positioner (Thermionics Northwest XY-B450/T275-1.39 precision XY manipulator + FLMM133 precision Z feed-through) is $10\ \mu\text{m}$. Thus the position of the cavity with respect to the MOT should be adjustable with precision of $10\ \mu\text{m}$ along the cell axis and with a precision of $2\ \mu\text{m}$ along the two other axes. To avoid eventual contact of the holder with the walls of the chamber or glass cell which might lead to jamming and damage, the positioner features a customizable travel limit. We were able to test the function of the holder and positioning of the cavity. The cavity could be moved along all three axes and fixed to a defined position.

The alignment of the dipole trap beam through the slit between the mirrors is a critical point. Since the mirrors are curved, the slit is smaller than the measured effective resonator length L . Knowing the mirror surface radius r and the radius of curvature R_c (see fig. 2.1) one can calculate its size d_{slit} :

$$d_{\text{slit}} = L - 2(R_c - \sqrt{R_c^2 - r^2}) \approx L - \frac{r^2}{R_c}.$$

For $r = 0.5\ \text{mm}$, $R_c = 10\ \text{mm}$, the slit is $25\ \mu\text{m}$ smaller than the resonator. For $L = 92\ \mu\text{m}$ its size is $d_{\text{slit}} = 67\ \mu\text{m}$. The dipole trap laser has currently the waist diameter of $2w_0 = 40\ \mu\text{m}$, with the focus in the center of the cavity the beam size on the slit is then about $42\ \mu\text{m}$. First measurements showed that about 95% of the power of the beam can be put through the cavity slit and glass windows in the test chamber. The power absorbed by mirror edges causes a strong thermal expansion of the mirrors which makes the spectral lines shift by a distance of several transversal modes when the laser is switched on. This has to be further examined and optimized.

2.4 Conclusion

We have set up and characterized a cavity with a length $L = 92\ \mu\text{m}$ and a finesse $F = 118000$. The cavity was assembled on a holder which enables its integration into our main experimental setup.

To achieve the best performance in cavity QED experiments the $\frac{g^2}{\kappa\Gamma}$ parameter has to be maximal. The current resonator with $(g, \kappa, \Gamma) = 2\pi \cdot (40.3, 13.8, 5.2)\ \text{MHz}$ has the ability to achieve the strong coupling regime. To further improve the performance, one has to increase the coupling g and to decrease the photon loss rate κ . As we have seen in the previous section the high power conveyor belt laser has to fit through the slit between the mirrors and thus sets a lower boundary to the mirror distance. The current slit size of $d_{\text{slit}} = 67\ \mu\text{m}$ already causes problems with power absorbed by the mirrors. Thus the coupling rate g can not be increased. The only parameter which can be improved is κ , by increasing the mirror reflectivity. In this respect a quick and reliable method of characterizing mirrors before could be useful. Such a method will be presented in chapter 4.

Chapter 3

Active stabilization of the cavity

Cavity QED experiments require precise control of the cavity resonance frequency with respect to an atomic transition. This requires a very high mechanical stability of the resonator, since due to high finesse, fluctuations of the cavity length shift the resonance frequency by more than its width. The fluctuations are caused by thermal drifts and inevitable mechanical vibrations. The passive mechanical stability is not sufficient, an active feedback scheme is required to compensate for the fluctuations. In this chapter a scheme is presented which is capable of stabilizing the cavity length to a fraction of a picometer.

Active stabilization implies the use of a stable reference frequency (e.g. that of a laser). A servo loop then holds the cavity resonant with the laser thus stabilizing its resonance frequency to the laser frequency. In order to achieve this, an error signal must be extracted. This signal contains the information about magnitude and sign of deviation of the resonance frequency from the desired value. After suitable filtering and amplification the signal is fed back to the cavity. In our setup the extraction of the error signal is accomplished using the Pound-Drever-Hall method [Dre83].

3.1 Pound-Drever-Hall method

The basic idea of this method is to use the property of the laser beam reflected from the cavity to derive an error signal, see fig. 3.1. The phase of this reflection is dispersive, i.e. it changes sign around resonance. When the laser frequency matches the cavity resonance, the phase is zero; for small deviations it is proportional to the difference of the laser and cavity resonance frequencies. This property is used for an error signal, which can then be used to stabilize a cavity to a stable laser, or vice versa.

The PDH method extracts the relative phase of three different frequencies which will experience different phase changes. A PDH setup for stabilizing a cavity to a stable reference laser is shown in fig. 3.2. The laser frequency ω is modulated with the frequency Ω , generated by a local oscillator. The field amplitude of the modulated laser beam is then:

$$E(t) \propto \exp(i(\omega + \alpha \sin(\Omega t)t)).$$

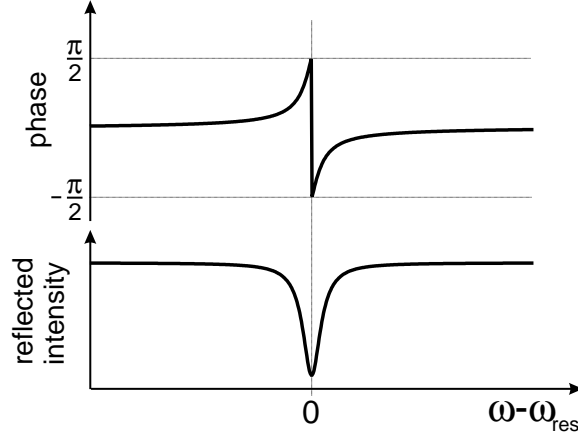


Figure 3.1: Intensity and phase of a laser field reflected from the cavity.

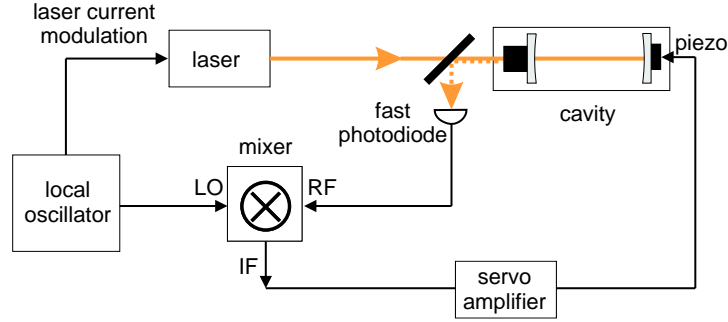


Figure 3.2: Basic PDH setup for stabilization of a cavity to a laser.

To first order it produces two sidebands with opposite phases at frequencies $\omega \pm \Omega$, for convenience we set the amplitudes of the sidebands equal to the carrier amplitude:

$$E(t) \propto e^{i\omega t} + e^{i(\omega+\Omega)t} - e^{i(\omega-\Omega)t}.$$

This laser field is sent to the cavity. The cavity has a free spectral range $\Delta\omega_{\text{FSR}}$ (which for small length changes can be considered constant), its resonance frequencies are $\omega_{\text{res}} = \Delta\omega_{\text{FSR}}q$, $q = 1, 2, \dots$. Suppose the laser frequency is near one of the resonances, we call the detuning of the laser frequency from the cavity resonance $\Delta\omega := \omega - \omega_{\text{res}}$. From eq. (1.1) we know

$$A(\Delta\omega) := \sqrt{R}T \frac{e^{i\frac{2\pi}{\Delta\omega_{\text{FSR}}}\Delta\omega}}{1 - R e^{i\frac{2\pi}{\Delta\omega_{\text{FSR}}}\Delta\omega}} - 1,$$

the complex response from the cavity. The reflected amplitude is then

$$E_r \propto A(\Delta\omega)e^{i\omega t} + A(\Delta\omega + \Omega)e^{i(\omega+\Omega)t} - A(\Delta\omega - \Omega)e^{i(\omega-\Omega)t}.$$

The resulting intensity is measured by a fast photo-detector:

$$I_r \propto E_r \cdot E_r^* \propto |A(\Delta\omega)|^2 + |A(\Delta\omega + \Omega)|^2 + |A(\Delta\omega - \Omega)|^2 + \\ + [A(\Delta\omega)A^*(\Delta\omega + \Omega)e^{-i\Omega t} - A(\Delta\omega)A^*(\Delta\omega - \Omega)e^{i\Omega t} - A(\Delta\omega + \Omega)A^*(\Delta\omega - \Omega)e^{i2\Omega t}] + \text{c.c.}$$

For phase detection, this signal is multiplied by the modulation frequency $e^{i(\Omega t + \gamma)}$, where γ is the phase of the local oscillator relative to the photodiode signal. The non-oscillating components of the result are:

$$(I_r e^{i(\Omega t + \gamma)})_{\text{DC}} \propto e^{i\gamma} (A(\Delta\omega)A^*(\Delta\omega + \Omega) - A^*(\Delta\omega)A(\Delta\omega - \Omega)) = \\ = e^{i\gamma} R \left(T \frac{e^{i\frac{2\pi}{\Delta\omega_{\text{FSR}}}\Delta\omega}}{1 - R e^{i\frac{2\pi}{\Delta\omega_{\text{FSR}}}\Delta\omega}} - 1 \right) \left(T \frac{e^{-i\frac{2\pi}{\Delta\omega_{\text{FSR}}}(\Delta\omega + \Omega)}}{1 - R e^{-i\frac{2\pi}{\Delta\omega_{\text{FSR}}}(\Delta\omega + \Omega)}} - 1 \right) - \\ - e^{i\gamma} R \left(T \frac{e^{-i\frac{2\pi}{\Delta\omega_{\text{FSR}}}\Delta\omega}}{1 - R e^{-i\frac{2\pi}{\Delta\omega_{\text{FSR}}}\Delta\omega}} - 1 \right) \left(T \frac{e^{i\frac{2\pi}{\Delta\omega_{\text{FSR}}}(\Delta\omega - \Omega)}}{1 - R e^{i\frac{2\pi}{\Delta\omega_{\text{FSR}}}(\Delta\omega - \Omega)}} - 1 \right).$$

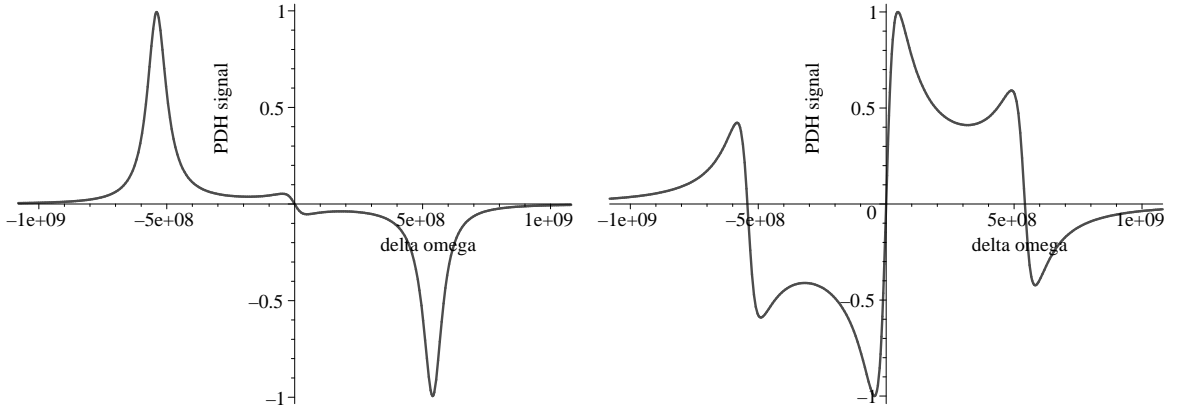


Figure 3.3: Real part of PDH signal for $\gamma = 0.99 \cdot \pi$ (left) and $\gamma = \frac{1}{2}\pi$ (right) vs. the relative detuning $\Delta\omega$.

The real part of the resulting signal is shown in the figure 3.3. Around $\Delta\omega = 0$ it has a dispersive feature which we want for the error signal. Its shape depends on the phase γ which is in experiment determined by the path length of the signals from the generator and photodiode to the mixer (multiplier). The steepest slope is obtained for $\gamma = \frac{\pi}{2}$; γ can be adjusted by varying the cable length from the local oscillator to the mixer.

The resulting error signal can be used for stabilization. After necessary amplification it is applied to the cavity piezo, closing the feedback loop. This loop (lock) stabilizes the resonance frequency of the cavity to the laser frequency. Since the signal depends only on the difference of

the laser and cavity frequencies, one can use it as well for stabilizing the laser frequency to the resonance of a stable cavity.

For the case $\gamma = \frac{\pi}{2}$ we are interested in the steepness of the slope. For $\Delta\omega \ll \Omega$ and small cavity linewidth (high finesse) the sidebands are far from the cavity resonance and thus

$$\frac{e^{\mp i \frac{2\pi}{\Delta\omega_{\text{FSR}}}(\Delta\omega \pm \Omega)}}{1 - R e^{\mp i \frac{2\pi}{\Delta\omega_{\text{FSR}}}(\Delta\omega \pm \Omega)}} \rightarrow 0.$$

Furthermore we note that for $\Delta\omega$ near 0 one obtains in the first order

$$\frac{T e^{\pm i \frac{2\pi}{\Delta\omega_{\text{FSR}}}\Delta\omega}}{1 - R e^{\pm i \frac{2\pi}{\Delta\omega_{\text{FSR}}}\Delta\omega}} \approx \frac{T(1 \pm \frac{2\pi}{\Delta\omega_{\text{FSR}}}\Delta\omega)}{(1 - R)^2} \cdot (\pm R \frac{2\pi}{\Delta\omega_{\text{FSR}}}\Delta\omega).$$

Setting $T = 1 - R$ for the case of no losses, the linear part of the signal near resonance is

$$PDH(\Delta\omega \ll \Omega) = 4 \frac{\Delta\omega}{\Delta\omega_{\text{FWHM}}}. \quad (3.1)$$

As expected, the sensitivity of the error signal increases with decreasing linewidth. This means that a high finesse cavity produces a more sensitive error signal and can be stabilized more accurately.

3.2 Stabilization setup

For the application of the PDH method for cavity stabilization a stable reference laser is required. One possibility would be to use the laser at 852 nm, which is stabilized to a atomic resonance. But the presence of such a laser within the cavity would continuously excite the atom and thus disturb its interaction with the cavity mode. Continuous stabilization requires a far detuned lock laser at low intensity which interacts only weakly with the atoms inside the cavity.

Therefore a stable laser is required which is far detuned from the 852 nm Cs resonance. In order to provide accurate stabilization, the mirrors should still have a high finesse for this laser, see eq. (3.1). This limits the possible detuning to few tens of nm. There is no simple method of stabilizing the laser to an atomic resonance in this wavelength range (e.g. Rb D_1 , 794 nm is already too far away). Our way to solve this problem is to take a laser at 836 nm and to stabilize it to the stable resonant 852 nm laser via an additional (transfer) cavity. This solution incorporates a “chain” of 3 locks.

The figure 3.4 shows a simplified scheme of the lock chain. It begins with the resonant “probe” laser which is already stabilized to the atomic transition by means of polarization spectroscopy and serves as a stable reference for the lock chain.

In the first step the probe laser stabilizes the transfer cavity. The laser is phase modulated with an EOM at 20 MHz and its reflection off the cavity is detected with PD1.

The second step is the stabilization of the lock laser. The sidebands are produced by a direct modulation of the laser diode current at 86 MHz. The reflection of the lock laser from the transfer

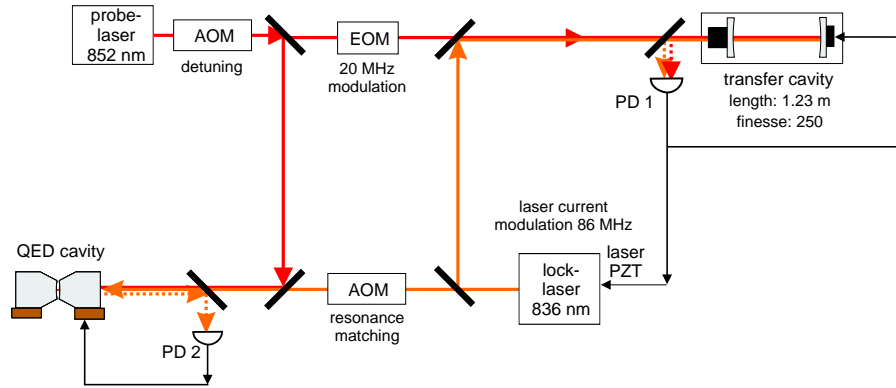


Figure 3.4: Stabilization scheme of the QED cavity using an off-resonant lock laser. PDH electronics are omitted.

cavity is detected by the same detector PD1. Since the modulation frequencies of the two laser beams are different, the two signals do not interfere.

Finally, the lock laser is used for stabilization of the QED cavity. The frequency modulation is the same 86 MHz as for the stabilization of the lock laser itself and is detected with PD2.

Before entering the QED cavity the lock laser passes an additional AOM. This AOM shifts the frequency of the lock laser to match the QED cavity resonance. When the transfer cavity is stabilized to the probe laser its resonance frequencies are fixed. Since the lock laser is continuously tunable with the current within a wide range, one can tune it into resonance with the transfer cavity. But at the same time it must be resonant with the QED cavity whose resonance frequency is defined by the atom. The solution is the big length of transfer cavity (1.23 m) which leads to a free spectral range of only about 120 MHz. Then one can find a lock laser frequency which is resonant with the transfer cavity and at most 60 MHz away from the QED cavity resonance. This remaining gap is bridged by the AOM.

This setup was already implemented in the previous work [Mir02]. It was shown that the individual stabilizations work, but the system was not tested as a whole.

3.3 Improvement of the stabilization system

In order to achieve the performance of the stabilization system which is required by future cavity QED experiments, several problems had to be overcome. The two most important issues were the mechanical resonance of the piezo elements and the reduction of the necessary lock laser power in order to minimize its influence upon the atoms in the QED cavity.

3.3.1 Compensation of resonances

Resonances in the response of a feedback loop can be either electrical (between some parasitic capacitances and inductivities) or mechanical. At a resonance the gain profile of the feedback loop has a π phase jump, which causes oscillations of the loop. Additionally, any driving (including noise) at the resonance frequency is enhanced by a large factor. We encountered a significant mechanical resonance of the piezo elements at a frequency of 40 kHz.

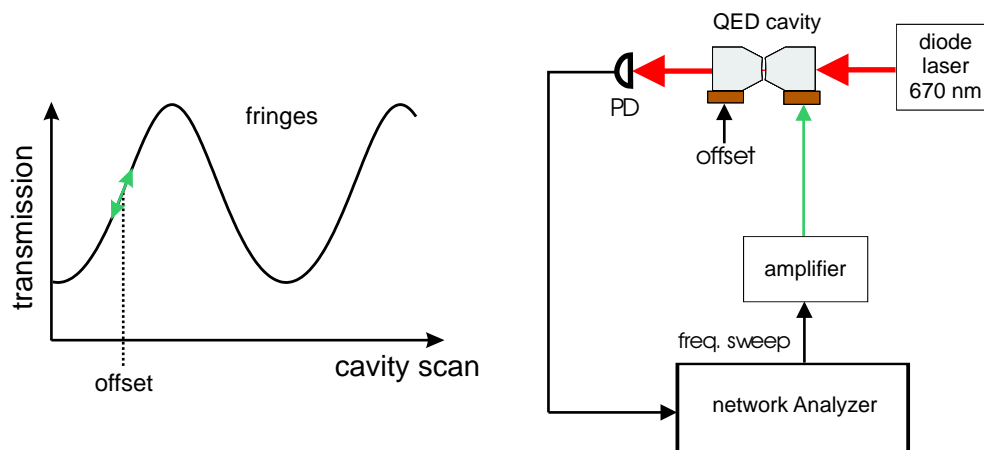


Figure 3.5: Setup for measuring the piezo resonance. The interference fringes of the cavity transmission provide a measure for the response of the piezo to a given signal.

In order to measure the frequency response of the piezo element we used the setup shown in fig. 3.5. A beam of a diode laser (670 nm) is sent through the cavity. For this wavelength the mirrors are practically transparent (only few % reflection). Thus, by scanning the cavity one observes broad interference fringes instead of narrow resonance lines. Applying a voltage offset to one piezo one can set the working point at the slope of a fringe.

After this, a small signal of a certain frequency is applied to the other piezo. The changes in the transmitted intensity are then proportional to the displacement of the mirror. The advantage of a far detuned laser is that these changes are not as sensitive as a resonance line. The response can be measured automatically with the help of a network analyzer. This device generates a sweep of frequencies, injects it into a given “network” and measures the amplitude and phase of the output for each frequency. Figure 3.6 shows the power spectrum around the resonance. The resonance has a significant enhancement of about 30 dB at 40 kHz.

Once the parameters of the resonance are known, the task is to compensate it. The resonance is an intrinsic property of the piezo element due to its geometry and material. Changing the shape of the piezo elements is not an option with an assembled resonator and also would only change the resonance frequency but not avoid it completely. The only way of compensation is to reduce the gain of the feedback loop in the range of resonant enhancement by electronic means.

One possible solution is to use a low-pass filter, cutting off all frequencies near and above the resonance. The disadvantage is that it limits the bandwidth of the feedback loop. A better way is

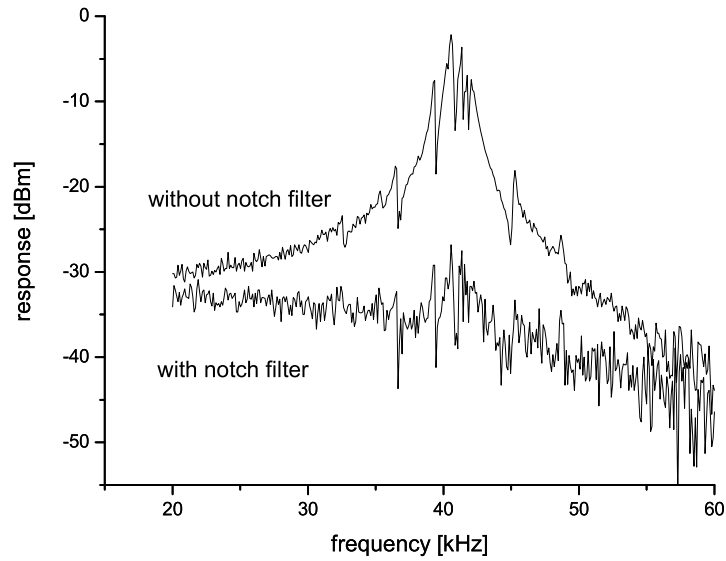


Figure 3.6: Resonance of the piezo element. The upper curve shows the response of the piezo. The lower curve shows the response compensated with a notch filter.

the use of a so called notch filter. This filter blocks frequencies only within a certain range. We use a simple passive design shown in the figure 3.7.

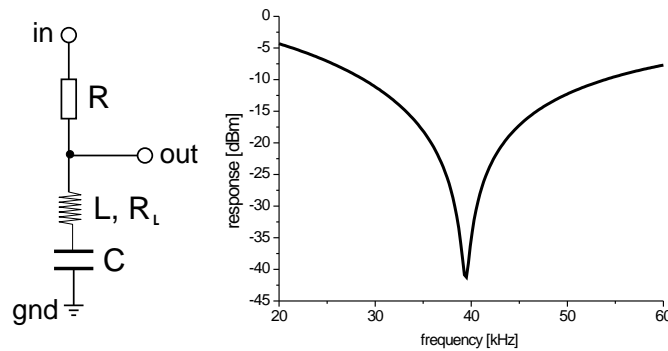


Figure 3.7: Schematic of a notch filter and calculated frequency response for the parameter set $R = 470 \Omega$, $L = 1 \text{ mH}$, $C = 16.3 \text{ nF}$, $R_L = 4 \Omega$.

The idea is to use a series LC circuit, where the resonance of the coil and capacitor makes their joint resistance go to zero for a defined frequency ω_{res} . The condition for the resonance is

$$i\omega_{\text{res}}L - \frac{i}{\omega_{\text{res}}C} \stackrel{!}{=} 0 \Rightarrow \omega_{\text{res}} = \frac{1}{\sqrt{LC}}$$

The residual resistance is given by the ohmic resistance R_L of the coil. It determines the resonant

damping factor and the width of the resonance. The damping is given by:

$$\frac{U_{\text{out}}(\omega = \omega_{\text{res}})}{U_{\text{out}}(\omega = 0)} = \frac{R_L}{R}.$$

Inserting the filter after the high voltage amplifier before the piezo element removes all 40 kHz signals, including noise of the amplifier. We have chosen the parameters:

$$R = 470 \Omega, L = 1 \text{ mH}, C = 16.3 \text{ nF}.$$

The coil has an intrinsic resistance of $R_L \approx 4 \Omega$. Figure 3.6 shows the response with the notch filter; the resonance is very well compensated.

To reduce minor electrical resonances we have added a resistor (10 k Ω) in series with the piezo element. Its purpose is to damp the resonances of the piezo capacitance and inductivities in the amplifier and cables. These resonances usually have high frequencies, but still influence the feedback. The resistor reduces their Q factors making the gain profile of the feedback loop smoother. The complete loop is shown in the fig. 3.8.

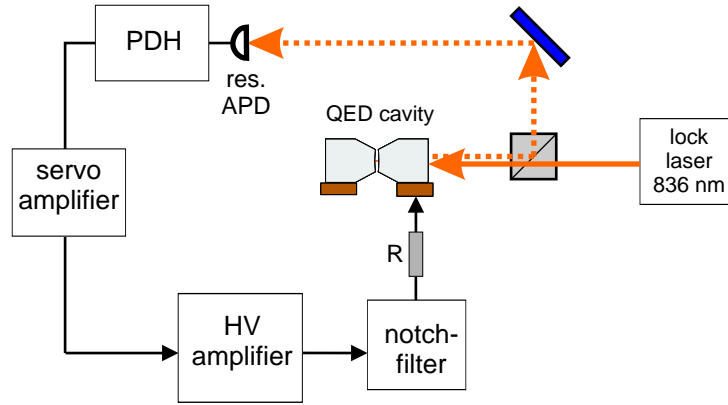


Figure 3.8: QED cavity lock with resonance compensation.

3.3.2 Resonantly amplified APD

The laser stabilization of the QED cavity must operate without disturbing the actual experiment. This limits the maximal power of the lock laser which can be present within the cavity before its influence upon the atoms becomes significant despite its detuning. One criterion is that atoms should not scatter more photons of the lock laser than of the dipole trap laser (which is inevitable for transporting the atoms into the cavity). The detuning Δ of the lock laser (836 nm) from the atomic resonance (852 nm) is 13 times smaller than the detuning of the dipole trap laser (1064 nm). The scattering rate $\Gamma_{\text{sc}} \sim \frac{1}{\Delta^2}$ gains a factor of 169. Additionally, the intensity of the lock laser is enhanced within the cavity by the factor $\frac{2}{\pi}F$, see eq. (1.4). To be sure that the scattering criterion is fulfilled even for a finesse of $F = 500000$, the lock laser power must be

about $5 \cdot 10^7$ times smaller than the power of the dipole trap. For a 4 W dipole trap, the limit is 80 nW. This requires a sensitive detector with a high signal-to-noise ratio.

We decided to use a resonantly amplified APD. This is an avalanche photo-detector with frequency selective amplification. The output signal of the detector is sent to an LC circuit which is tailored to be resonant with the Pound-Drever-Hall modulation frequency of 86 MHz. This makes the detector sensitive especially to this frequency, and at the same time suppresses all other signal sources at other frequencies, especially noise.

The performance of the home-built resonant APD prototype was compared to the previously used commercial photo-detector (Newport amplified silicon PIN, 818-BB-21A). With a 400 nW laser power the commercial photo-detector produces an error signal with a signal-to-noise ratio of 1. The stabilization worked insufficiently under such conditions.

The resonant APD, however, is able to perform a lock with less than 200 nW coupled into the fundamental mode of the cavity and less than 100 nW at the detector. The final version of the detector will have an improved electronics part and it will also use a photodiode with better characteristics. With these improvements it will fulfill the requirement of low lock laser power for future cavity QED experiments.

3.4 Performance of the stabilization system

After implementation of the improvements described above, the lock chain is finally complete and we are interested in the resulting performance. As we have already seen, the requirements for the system are:

- frequency stability: the residual fluctuations of the cavity resonance frequency must be well below the linewidth
- low lock laser intensity: to keep the influence on the atoms small, the lock laser power at the cavity should be below 80 nW
- robustness: the lock should be able to withstand considerable external distortions, including the thermal effect of the dipole trap laser

In this section we present the current state of the system.

3.4.1 Characterization of the chain of locks

Our method to measure the frequency stability is to observe the fluctuations of the error signal while the feedback loop is active. They are directly related to the resonance frequency fluctuations. For this measurement one scans the cavity and displays simultaneously the error signal and the transmission of the corresponding laser on an oscilloscope. One measures the width of the transmission line together with the slope of the error signal, see fig. 3.9. These two values allow us to relate the error signal to the frequency deviation. Finally the stabilization is activated and the residual root-mean-square (rms) fluctuations of the error signal are measured. With the

known linewidth it is then possible to determine the real cavity resonance frequency fluctuations via the fluctuations of the error signal.

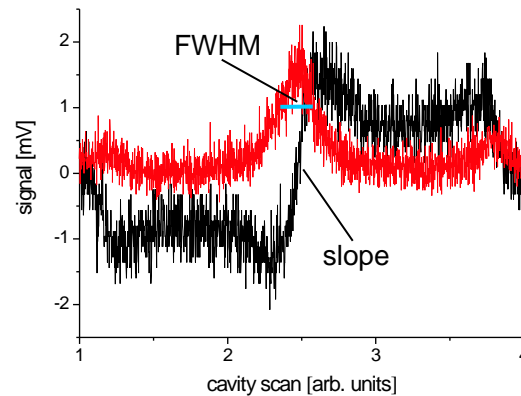


Figure 3.9: Transmission and error signal of the QED cavity at 200 nW lock laser power.

The lock chain was characterized according to the procedure described above. We began with the lock of the transfer cavity to the probe laser. Then, the lock laser was measured with locked transfer cavity and, finally, the QED cavity with the rest of the lock chain active. We obtained the following values:

- Transfer cavity to the probe laser (linewidth 480 kHz):

frequency fluctuation rms: 32.6 kHz.

- Lock laser to the transfer cavity:

frequency fluctuation rms: 27.3 kHz.

- QED cavity to the lock laser (linewidth 16 MHz):

frequency fluctuation rms: 2 MHz (12.5% of FWHM).

which corresponds to resonator length fluctuations of only 450 fm.

The laser power used for the QED cavity stabilization was 200 nW coupled into the fundamental mode and 100 nW arriving at the resonant APD (see also fig. 2.5).

One should note that the given values depend on environmental conditions. Acoustical noise, vibrations, etc. increase the frequency fluctuations. The values were measured in a typical situation, with people working in the lab and various devices switched on. Additionally, the QED cavity lock suffers from 50 Hz noise as will be discussed later.

3.4.2 Scanning of the stabilized cavity

With the complete lock chain active one has the possibility to tune the lock laser frequency with an AOM before it enters the QED cavity. This is necessary to achieve any desired detuning of the locked cavity with respect to the atomic resonance. If the detuning process is slow enough, the cavity will follow the changing lock laser frequency while staying stabilized, see fig. 3.10.

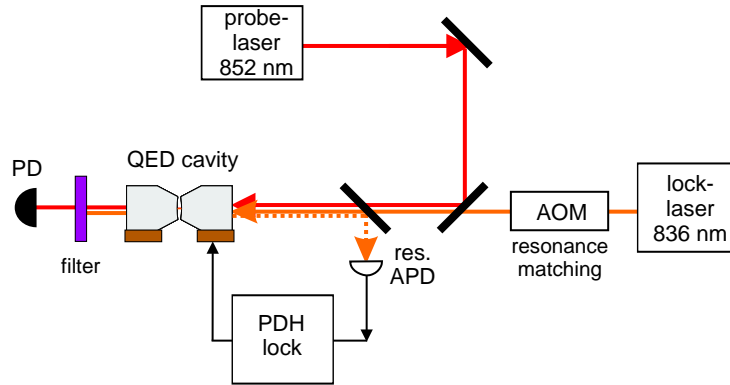


Figure 3.10: Scheme of cavity detuning. The locked cavity follows the detuning of the lock laser.

As a test of this statement we scanned the QED cavity over the probe laser line. In order to do this we adjusted the current of the lock laser such, that it was resonant with the transfer cavity and its line in the QED cavity was only few MHz apart from the probe laser line. Then the lock laser was stabilized to the transfer cavity and the QED cavity to the lock laser. Finally, by scanning the AOM we have scanned the stabilized QED cavity over the probe laser line with the frequency of 100 Hz. The probe laser transmission during this scan is given in fig. 3.11.

The scan range is not the full AOM range since the transmitted power is not constant over the detuning. Since the changing intensity of the lock laser changes the error signal offset it is not possible to maintain the lock under strong intensity variations ($\sim 50\%$).

The linewidth in this picture is about 20 MHz. It is larger than the 14 MHz measured earlier, and also the line shape is asymmetric, possibly due to strong averaging and limited photo-detector speed. Still, the system is able to compensate external perturbations even if scanned with 100 Hz over a 60 MHz detuning range for over 30 minutes.

3.5 Conclusion

The stabilization system was completed and optimized to match the experimental requirements. It is capable of reducing the resonance frequency fluctuations of the QED cavity to a few percent of its linewidth. The system works at 200 nW lock laser power already with the first prototype of the resonant APD. The required value of 80 nW for future cavities with higher finesse will be realized with the improved resonant APD. The lock is also able to restore the initial resonance frequency even after strong knocks on the optical table and loud acoustical distortions.

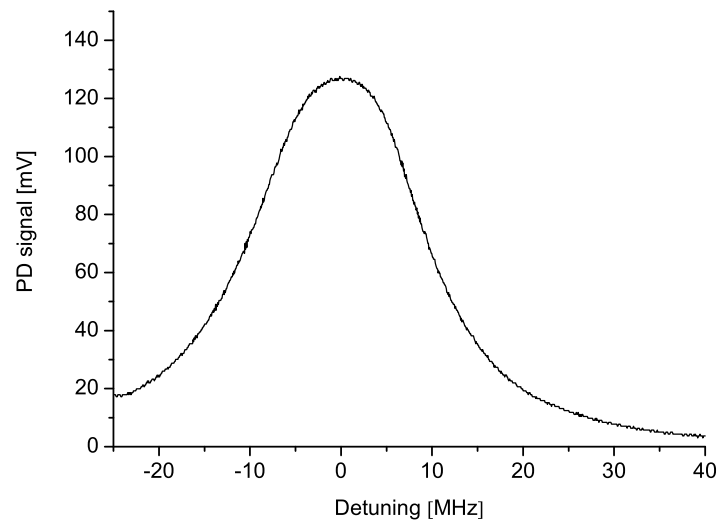


Figure 3.11: Scan of the locked cavity over the probe laser resonance. The scan rate is 100 Hz, the average of 64 tracks was taken.

One of the main problems is the effect of the conveyor belt laser. Having large power (4 W), even a small part of the beam absorbed by the mirrors disturbs the stabilization due to thermal effects. Preliminary experiments in the test chamber showed that the lock was unable to compensate for the mirror expansion when the laser was switched on. It has to be further considered.

Another issue remains the 50 Hz noise. It can be produced by practically any device in the lab and is induced electronically over ground loops. Being induced onto the error signal it causes periodic fluctuations of the resonance frequency on the order of 10% of the linewidth. A possible way to solve this problem is the proper grounding of all involved electronic devices. We grounded most of the devices in direct vicinity of the setup and switched off unnecessary ones, this reduced the noise but this issue still has to be improved.

Chapter 4

Cavity ring-down

In order to achieve the best experimental parameters for our cavity, we have to select mirrors with the best possible reflectivity. As we have seen, the characterization of the mirrors by measuring the linewidth requires a stable resonator and a time-consuming assembly process. In our case the mirrors are glued onto piezo elements and thus can not be reused. In view of the strong variations of the mirror quality, a quicker and simpler method for measuring the finesse would be of great advantage. In this chapter I present a method which enables us to quickly test the mirror finesse and sort out good mirrors *before* the resonator is assembled.

4.1 Basic principle

The task of measuring the finesse of a mirror pair is equivalent to measuring the photon lifetime within the cavity. Using an assembled resonator it was done by measuring the spectral linewidth together with the free spectral range, see sec. 2.2.3. However, this method requires a stable resonator, mechanical and electronic noise sources make the line move or change its shape. Another possibility to infer the finesse quickly, is to directly measure the photon lifetime by observing the decay of cavity transmission. The cavity is filled with photons by tuning it into resonance with the laser before we switch the laser off. The photons start to leak out and the cavity field decays exponentially. The time evolution of the intensity leaking out of the cavity is given by eq. (1.9):

$$I(t) = I(t=0)e^{-\frac{t}{\tau}},$$

where $\tau = \frac{1}{\kappa}$ is the (resonator length dependent) photon lifetime. As already shown in eq. (1.10), τ is directly connected to the finesse:

$$F = \Delta\omega_{\text{FSR}}\tau = \pi\frac{c}{L}\tau.$$

Thus, the observation of the intensity decay of the cavity transmission allows us to determine the time constant τ and the finesse F .

The main advantage of this method is its insensitivity to external perturbations. Mirror distance fluctuations of 10^{-5} fraction of the wavelength make the linewidth measurement difficult (see sec. 2.2.3). On the other hand, the lifetime change caused by such fluctuations is negligible because these length changes are small compared to the total cavity length. Therefore one does not need to stabilize the resonator for this measurement.

4.2 Setup

The experimental task is to couple the laser into the cavity, to switch it off and to observe the decay of transmission.

For this purpose I have built the setup is shown in fig. 4.1. The laser beam (852 nm) passes an AOM which serves as a fast switch. The beam is led to the setup via an optical single-mode fiber which additionally serves as a spatial mode filter. Two mirrors couple the laser beam into the cavity. The last element before the cavity is a lens ($f = 80$ mm) which mode matches the beam with the fundamental mode (waist $35\ \mu\text{m}$). The cavity transmission is observed by a camera and a fast APD, the observation optics consists of a lens ($f = 100$ mm). The camera is a simple compact CCD, it enables us to distinguish the different transversal modes. The APD has a bandwidth of 9 MHz, which is fully sufficient to perform measurements on a microsecond time scale.

The mirror distance is chosen to be 10 mm to ensure a lifetime in the range of microseconds which can be measured without especially fast detectors and electronics. Given the mirror curvature $R_c = 10$ mm, the waist of the fundamental mode is then $35\ \mu\text{m}$ and its radius on the mirror is about $50\ \mu\text{m}$.

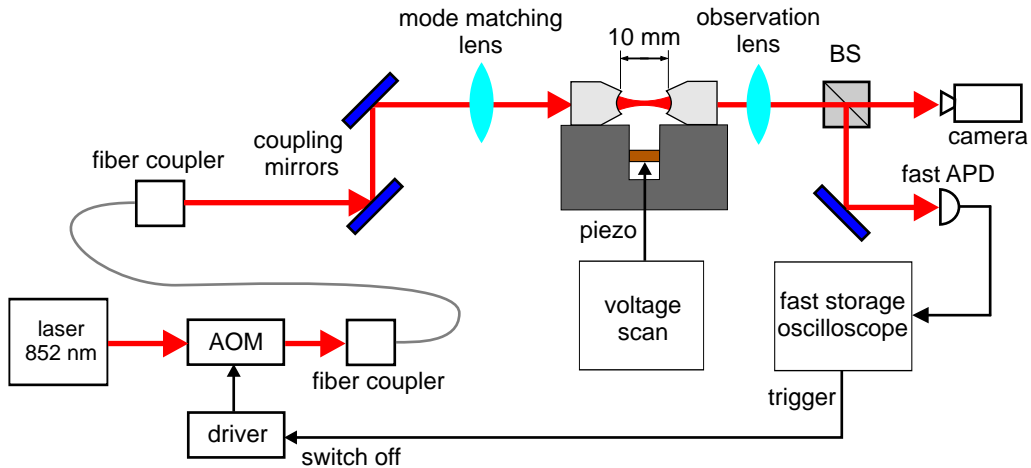


Figure 4.1: Cavity ring-down setup.

The whole optical setup except for the AOM fits on a 30x30 cm breadboard and is placed under a flow-box to avoid pollution of the mirrors. To avoid a set up of an additional AOM I used the laser and AOM from the cavity stabilization setup (fig. 3.4, “detuning” AOM).

4.2.1 Mirror holder

Special care was taken to design the mirror holder. In order to simplify the coupling into the mode it should be possible to place the mirrors coaxially without much effort. This can be achieved by putting them into a V-groove. Additionally, one must also be able to scan the mirror distance to tune the cavity in resonance with the laser.

The design and view of the holder are shown in fig. 4.2. It is an aluminum block in which a slit of 5 mm is cut. The slit almost cuts the whole block, only a small rest of metal holds the two halves together. On one side a small layer of the lower part is removed, such that this part can be tilted. In order to scan the mirror distance, a piezo element is fixed in the slit, which is able to push the two halves apart. This piezo element (Piezomechanik PSt 150/2x3/5) is pressed with a screw against one wall of the slit such that if the piezo contracts, the two halves approach. For better force transmission to the screw it has a spherical corundum end piece. The maximal stroke is $7\mu\text{m}$ for 150 V and with $\pm 10\text{V}$ one can scan about $1\mu\text{m}$ which covers two free spectral ranges.

The main part of the holder, the V-groove, is cut in the last fabrication step to go straight through both halves. Now the mirrors can be simply put into the groove and are lying coaxially, assuming their shape is well cylindrical. If the mirrors had to be placed on separate holders it would increase the degrees of freedom by 2×2 , making mode matching nearly a hopeless task. With our coaxially positioned cavity mirrors the mode matching is done using two mirrors while scanning the piezo voltage, which constitute 5 degrees of freedom in total.

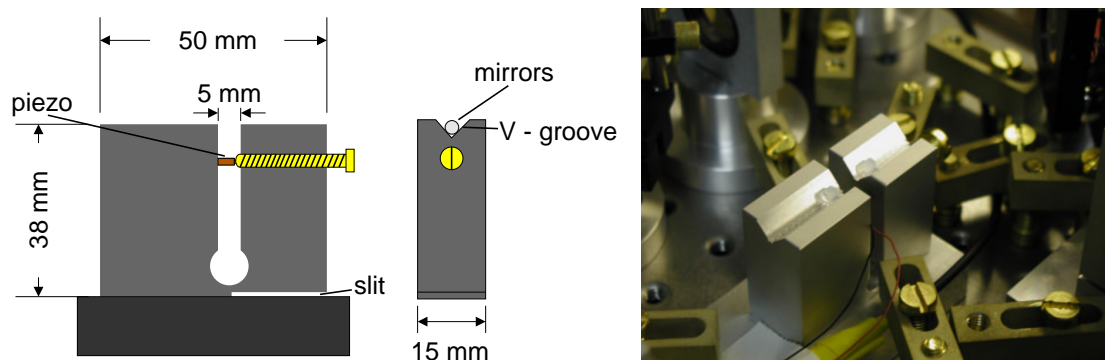


Figure 4.2: Holder for mirrors.

In order to scan the cavity we apply to the piezo a triangle signal with variable amplitude and offset (max. $\pm 10\text{V}$). By these means we can tune the cavity in resonance with the laser.

When putting mirrors into the holder their distance is set manually to 10 mm with the help of two reference marks on the side of the holder. This distance of 10 mm is also convenient, because $1\mu\text{s}$ decay time corresponds approximately to a finesse of 100000. The manual adjustment of the distance limits the precision of the finesse measurement to $\pm 5\%$, this will be discussed later.

4.2.2 Laser switching

In order to observe photon decay one has to bring the cavity in resonance with the laser and switch it off much faster than the photon lifetime. This is accomplished by scanning the cavity distance slowly (10 – 100 Hz) over the laser resonance, resulting in an increase of the transmission. The transmission signal of the APD is sent to a storage oscilloscope. When its level reaches some defined threshold, the oscilloscope generates a trigger signal. This signal is a standard TTL voltage step from 0 V to +5 V. It is sent to an inverting unit (DM74LS00 logical NAND) and becomes a step from +4 V to 0 V. This voltage is fed through an buffer amplifier (Buf634), which is a gain 1 amplifier for high power. Its output signal controls the driver (Neos N21125-1AMVCO) of the AOM (Neos 23125) which serves as a fast switch.

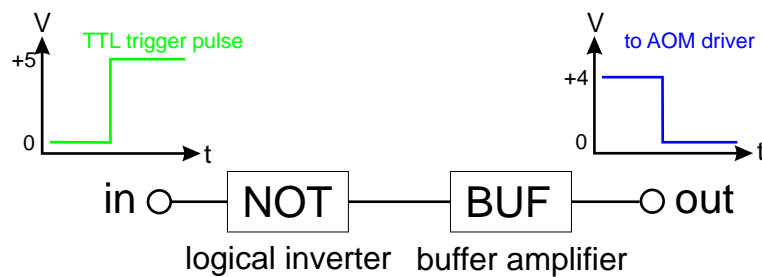


Figure 4.3: Inverter for laser switching.

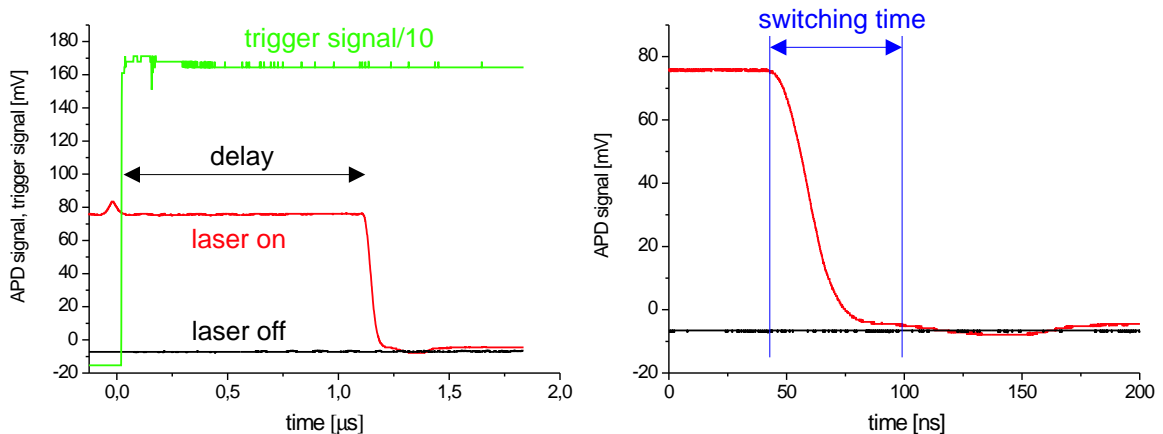


Figure 4.4: Laser switch-off behavior. Overview of the process on the left, zoom in on the right.

Figure 4.4 shows the switching process, taken without cavity. It shows the transmission signal of the APD and the signal one obtains without laser (zero level). Switching time below 100 ns is achieved, which is fully sufficient for our purpose. Two parameters influence the switching

time. First is the speed of electronics (inverter unit). The inverting unit was measured to give switching time below 25 ns. The second is the speed of the AOM driver and the relaxation in the AOM crystal itself. There a sonic wave creates a refraction index Bragg grating. This moving pattern diffracts the laser beam, the first order diffraction can be controlled by the power of the sonic wave. After the power is switched off, the grating starts to fade. The fading crosses the site of the beam focus at the sonic velocity. For typical parameters of $30\mu\text{m}$ waist and $3\frac{\text{km}}{\text{s}}$ sonic velocity it takes about 20 ns for the wave to traverse the focus.

One can see the delay of about $1\mu\text{s}$ between the trigger signal and the beginning of the switching process. It results from the fact that the fading has to traverse a part of the crystal (few mm) to reach the beam focus site. Additionally there is a small run time in the cables. The laser is not completely extinguished, there is a residual intensity of less than 3%. This is due to voltage offset produced by the inverting unit, such that the AOM control voltage does not go to zero.

Additionally the APD produces a negative offset of 7 mV. Another feature is that the transmission signal at some point falls below the zero level. This is due to the APD which has a bandwidth of 9 MHz and is working at its speed limit in this case. During the actual experiment with fall off times in a microsecond range this effect does not occur.

4.3 Measurements

4.3.1 Procedure

After the mirrors are put into the holder, there are two tasks to accomplish: mode matching and the observation of decay.

Mode matching: We work with the fundamental mode of the cavity, which illuminates a well defined spot on the mirror surface in a homogeneous way. In order to do this we need to couple most of the intensity into this mode to ensure high transmission. It is achieved by means of two mirrors placed before the resonator and controlling beam position and angle. The transmission is observed with a camera making possible to distinguish between the different transversal modes.

Practically, we switch to a small scan range and slow scan rate (at 10 Hz the eye can see even weak mode transmission blinks). We change the offset slowly, moving through the free spectral range and observing the transmission with the camera. Usually at least one higher transverse mode should be visible without adjustments. Then we can optimize this mode using one mirror and look in its vicinity for the neighboring lower transversal mode. We optimize this mode and moves on. By these means one can proceed to the fundamental mode. The scan is switched to 100 Hz and the fundamental mode coupling is then optimized with both mirrors.

This procedure requires some experience, the time needed for one measurement strongly depends on how easy one can find and optimize the fundamental mode. Typical times range between 5 and 20 minutes.

Observation of ring-down: After optimizing the coupling, the trigger of the storage oscilloscope is set to a possibly high value. This means that the transmission of the fundamental mode when scanning over the resonance should hardly reach this level. This provides a high signal

level and also the other modes do not trigger the measurement. Each time the transmission goes beyond trigger level the laser is switched off. The decay of the transmission is recorded with the storage oscilloscope and averaged over 64 measurements to increase the signal to noise ratio. Recording 64 decay curves takes less than one minute.

Accumulating and taking the mean value over several measurements with (in principle) varying intensity and trigger time is possible because of the properties of the exponential:

$$I_1 e^{-\frac{t}{\tau}} + I_2 e^{-\frac{t}{\tau}} = (I_1 + I_2) e^{-\frac{t}{\tau}}$$

and

$$I e^{-\frac{t-t_0}{\tau}} = I e^{-\frac{t_1-t_0}{\tau}} \cdot e^{-\frac{t-t_1}{\tau}} = I' e^{-\frac{t-t_1}{\tau}}.$$

Therefore the measurement of the time constant is not influenced by the absolute intensity and the time of the trigger. The residual intensity of the laser produces a (constant) offset which is again of no importance for the measurement.

4.3.2 Analysis

Figure 4.5 shows a typical measured decay curve, averaged over 64 measurements. The trigger signal is sent at $t = 0$ and after about $1 \mu\text{s}$ the transmission begins to decay. As expected, the decaying part of the curve has an exponential shape.

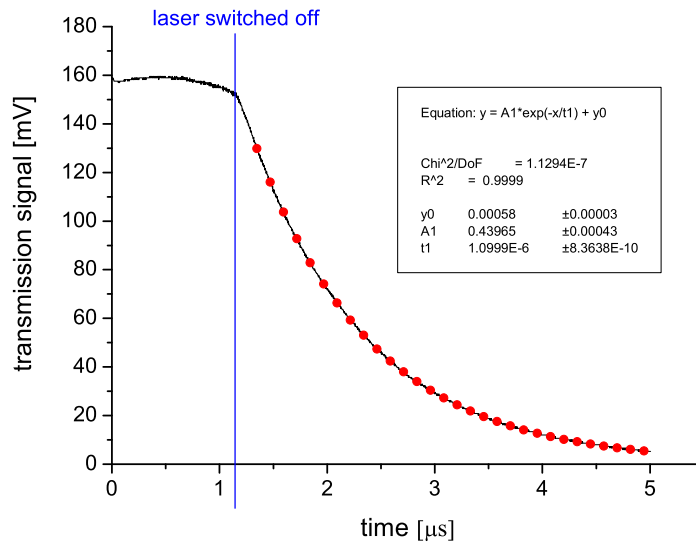


Figure 4.5: Decay of the transmission. The big points show the exponential fit.

We fit a function of the form $f(t) = A \cdot e^{-\frac{t}{\tau}} + y_0$ to the decay, where y_0 counts for the APD offset and residual laser intensity. The range of the fit begins about 500 ns after the switch-off

to exclude the switching process and to observe pure decay. The resulting quality of the fit is extremely high and does not limit the precision as we will see later.

4.3.3 Precision limits and reproducibility

In the following we will consider the factors which influence the measurement the lifetime.

- **Mirror distance:** Since the distance of 10 mm between the mirrors is adjusted manually with the help of reference marks on the holder, variations on the distance will occur. To estimate this error, the decay time τ was measured several times, one mirror being moved a bit and then readjusted again to the 10 mm distance.

#	1	2	3	4	5	$\bar{\tau}$	σ
τ [ns]	855	833	833	883	942	869.2	40.7

Table 4.1: Distance reproducibility measurement ($\beta B3$ vs $\beta A3$).

One can see that the reproducibility in this case is pretty high. The standard deviation of this set is $\sigma = 40.7$ ns which is about 5% of the mean value. This corresponds to length deviation of 0.5 mm. Still, this is the main limit of the precision of the finesse measurement, since the fit error is order of a magnitude smaller.

- **Mirror rotation:** If the mirrors are not perfectly coaxial within the groove, the mode is not exactly centered. Thus the mirror rotation exposes a different spot on the surface. Our experience with these mirrors shows, that the surface quality is extremely inhomogeneous (scratches, dust particles, etc.). The measurement below shows an example of repeated measurements after rotations of one of the mirrors (about 30°).

#	1	2	3	4	5	$\bar{\tau}$	σ
τ [ns]	925	886	913	354	806	776.8	215.4

Table 4.2: Measurement with rotation of one mirror, mirror pair $\beta B3$ vs $\beta A3$.

The large spread in the values shows that different spots of the mirror surface have different quality. Since the mirrors are not exactly coaxial, the rotation of one mirror moves the position of the surface a bit, which can also be seen with the camera. The resulting difference in finesse can be larger than 50% for a mirror pair. It can be due to the presence of single larger dust particles on the surface within the mode, but also a larger number of small spots may have the same effect.

We repeated the measurement with another mirror pair. Here the spread is very small and lies within the length precision. These mirrors have better finesse together a better homogeneity.

#	1	2	3	4	5	$\bar{\tau}$	σ
τ [ns]	1020	1019	1050	1064	1119	1054.4	36.6

Table 4.3: Measurement with rotation for the mirror pair $\beta D3$ vs $\beta B3$.

One important observation is the correlation of transmission and finesse: in most cases high transmission was accompanied by better finesse. The absolute transmission depends on the degree of mode matching, so this effect was not observed systematically. On the other hand mirror pairs with low transmission usually show relatively low finesse. This indicates that the dominating factor for the finesse are the losses. These could be either inherent (within the coating) or due to surface damage or pollution.

4.3.4 Characterization of a mirror set

Now we apply the method to our set of mirrors. We possess 18 mirrors which were cleaned by the manufacturer. We divided them into 3 sets of 6 mirrors, each set in a separate box. The boxes contain 5x5 grid of holes where mirrors can be placed. The boxes are signed α , β , γ and the grid chess-board-like A-E, 1-5.

The first step is to inspect the mirror surface with the help of a microscope (500x, dark-field). This is necessary to find a mirror with as homogeneous surface as possible. This mirror can then be used as a reference, i.e. we can measure all the other mirrors with this one. Finesse variations due to different mode spot positions will then mostly depend on the other tested mirror. Another reason for visual inspection is to try finding the dependence of measured finesse on visible surface condition. The inspection showed that most of the mirrors have many small spots and/or scratches in the center region (radius ~ 0.25 mm). Many of them had even macroscopic particles. All mirrors had at least a few spots in the center. According to our previous criteria of the old visual method even the best mirrors are imperfect. Still we found a mirror with only few spots in the center region which also were more or less equally distributed. We took this mirror ($\beta E3$) as a reference.

In the box β each of the five remaining mirrors was tested with the reference mirror 4 times, rotating the mirror after each measurement. The mirrors with the best performance in this test were then measured together. The results are shown in tab. 4.4.

As discussed above, the error of this measurement is about 5%. We see, that the mirror $\beta E3$ showing good surface quality which was chosen as the reference does not have the best finesse in this case. This shows that the visual inspection of the mirror surface gives only a coarse measure for the finesse.

Then we tested the boxes α and γ versus the reference mirror. The results are given in the tables. As one can see, 10 out 18 mirrors are far below the specification of 100000. If it is due to bigger dust particles on the surface which were visible under the microscope, the situation may be improved by cleaning.

The pair ($\alpha E1$, $\alpha D2$) yields a finesse of 180000. This is 50% better than the mirrors which are currently assembled in our test vacuum setup.

	$\beta A3$	$\beta B3$	$\beta C3$	$\beta D3$	$\beta E3$	$\beta A4$
$\beta A3$					83500	
$\beta B3$					94100	
$\beta C3$					98500	
$\beta D3$			111900		108500	117000
$\beta E3$					-	
$\beta A4$					89200	

Table 4.4: Best finesse for mirror set β

	$\alpha A1$	$\alpha C1$	$\alpha E1$	$\alpha B2$	$\alpha D2$	$\alpha A3$	$\beta E3$
$\alpha A1$							106400
$\alpha C1$							44600
$\alpha E1$					182900		111000
$\alpha B2$							46900
$\alpha D2$							131800
$\alpha A3$							51500

Table 4.5: Best finesse for mirror set α

	$\gamma A1$	$\gamma C1$	$\gamma E1$	$\gamma B2$	$\gamma D2$	$\gamma A3$	$\beta E3$
$\gamma A1$							82400
$\gamma C1$							111200
$\gamma E1$							81200
$\gamma B2$							63200
$\gamma D2$							51500
$\gamma A3$		118900					103900

Table 4.6: Best finesse for mirror set γ

Conclusion

I have implemented a compact and easy to use setup for fast mirror characterization. It is capable of measuring the mirror finesse quickly and with precision of about 5%. Applying it to the set of our mirrors I found a mirror pair with a considerably better finesse, than we currently have in our assembled resonator. The process of finding good mirrors for future resonators will be fast and reliable.

Summary and outlook

The goal of this work was to prepare a high finesse optical resonator for cavity QED experiments. The preparation includes finding mirrors of best reflectivity, building and characterizing the resonator and achieving the necessary stability for future experimental conditions.

Considering the amount of work for visually inspecting the mirrors and assembling the resonator we needed a method to characterize the mirrors quickly. I have implemented the setup for cavity ring-down, which measures the lifetime of photons in the cavity. It has the advantage that it does not require a stable assembled resonator. Instead, the mirrors are put into a specially designed holder which allows to align them reducing the amount of work substantially. With this setup we characterized our whole mirror set within a short time. It allows us to sort out mirrors with the best reflectivity and will be of a great advantage for setting up new resonators.

We have set up and characterized a resonator with length $L = 92 \mu\text{m}$ and finesse $F = 118000$. The obtained parameter set is $(g, \kappa, \Gamma) = 2\pi \cdot (40.3, 14, 5.2) \text{ MHz}$, which means that we can achieve the regime of strong coupling where the coherent atom-photon interaction g is larger than the incoherent loss processes κ, Γ .

Continuing the work of Y. Miroshnychenko [Mir02], we completed, optimized and characterized the cavity stabilization scheme. We have solved the problem of mechanical resonances of the piezo elements and implemented the resonantly amplified APD which is a highly sensitive detector for stabilization purposes. Finally we have shown that the system is able to stabilize the cavity to 12% of the linewidth under conditions of low lock laser power (200 nW).

The next steps will be the placement of the cavity into the main setup and transport of an atom into the cavity. The detection of an atom in the resonator can be performed by a measurement of the Rabi splitting of atom and cavity resonances. A major difficulty of this experiment will be the alignment of the conveyor belt laser which must fit through the small slit between the mirrors and connect the MOT with the cavity mode which have both a size of only about $30 \mu\text{m}$ and are 5 mm apart. Finally, after the deterministic transport of two atoms into the cavity mode, we will be able to realize a controlled atom-atom interaction which is a step towards a quantum logic gate.

Appendix A

Solution of the master equation

Enter the matrix

We begin with the master equation (1.13).

$$\frac{d}{dt}\hat{\rho} = \frac{1}{i\hbar}[\hat{H}, \hat{\rho}] + \frac{\kappa}{2}(2\hat{a}\hat{\rho}\hat{a}^\dagger - \hat{a}^\dagger\hat{a}\hat{\rho} - \hat{\rho}\hat{a}^\dagger\hat{a}) + \frac{\Gamma}{2}(2\hat{\sigma}\hat{\rho}\hat{\sigma}^\dagger - \hat{\sigma}^\dagger\hat{\sigma}\hat{\rho} - \hat{\rho}\hat{\sigma}^\dagger\hat{\sigma}),$$

with

$$\hat{H} = \hbar(\omega_0 - \omega_l)\hat{\sigma}^\dagger\hat{\sigma} + \hbar(\omega_c - \omega_l)\hat{a}^\dagger\hat{a} + \hbar g(\hat{\sigma}^\dagger\hat{a} + \hat{\sigma}\hat{a}^\dagger) + \hbar\varepsilon(\hat{a}^\dagger + \hat{a}).$$

Now we use the **weak field approximation**. In this regime the driving field ε is so small, that at most one excitation in the system is present. Therefore we consider only three states of the system:

$$|g\rangle|1\rangle, \quad |e\rangle|0\rangle, \quad |g\rangle|0\rangle.$$

Here, $|g\rangle$, $|e\rangle$ are the atomic ground and excited state, $|0\rangle$, $|1\rangle$ are states with zero and one photon in the cavity.

Calling these states 1, 2, 3 respectively, we define the 3 by 3 density matrix:

$$\begin{pmatrix} \rho_{11} & \rho_{12} & \rho_{13} \\ \rho_{21} & \rho_{22} & \rho_{23} \\ \rho_{31} & \rho_{32} & \rho_{33} \end{pmatrix}.$$

This matrix is Hermitian, i.e. $\rho_{mn} = \rho_{nm}^*$.

The corresponding creation and annihilation operators are:

$$\hat{a}^\dagger = |g\rangle|1\rangle\langle g|\langle 0| = \begin{pmatrix} 0 & 0 & 1 \\ 0 & 0 & 0 \\ 0 & 0 & 0 \end{pmatrix}, \quad \hat{a} = |g\rangle|0\rangle\langle g|\langle 1| = \begin{pmatrix} 0 & 0 & 0 \\ 0 & 0 & 0 \\ 1 & 0 & 0 \end{pmatrix},$$

$$\hat{\sigma}^\dagger = |e\rangle|0\rangle\langle g|\langle 0| = \begin{pmatrix} 0 & 0 & 0 \\ 0 & 0 & 1 \\ 0 & 0 & 0 \end{pmatrix}, \quad \hat{\sigma} = |g\rangle|0\rangle\langle e|\langle 0| = \begin{pmatrix} 0 & 0 & 0 \\ 0 & 0 & 0 \\ 0 & 1 & 0 \end{pmatrix}.$$

The dissipation in the system leads to a **stationary state** with

$$\frac{d}{dt}\hat{\rho} = 0.$$

This leads to a system of 9 homogeneous complex equations from which 6 are independent:

$$-\kappa\rho_{11} + i(g(\rho_{12} - \rho_{12}^*) + \varepsilon(\rho_{13} - \rho_{13}^*)) = 0$$

$$-ig(\rho_{12} - \rho_{12}^*) - \Gamma\rho_{22} = 0$$

$$\kappa\rho_{11} + \Gamma\rho_{22} - i\varepsilon(\rho_{13} - \rho_{13}^*) = 0$$

$$-\frac{1}{2}(\Gamma + \kappa)\rho_{12} + i(g(\rho_{11} - \rho_{22}) - \varepsilon\rho_{23}^* + (\omega_0 - \omega_c)\rho_{12}) = 0$$

$$-\frac{\kappa}{2}\rho_{13} + i(\varepsilon(\rho_{11} - \rho_{33}) - g\rho_{23} - (\omega_c - \omega_l)\rho_{13}) = 0$$

$$-\frac{\Gamma}{2}\rho_{23} + i(-g\rho_{13} + \varepsilon\rho_{12}^* - (\omega_0 - \omega_l)\rho_{23}) = 0.$$

Now we separate the real and imaginary parts, $\rho_{mn} = R_{mn} + iI_{mn}$, getting 9 real equations, which can be written as a matrix:

$$\begin{pmatrix} \frac{\kappa}{2} & 0 & 0 & 0 & g & 0 & \varepsilon & 0 & 0 \\ 0 & \frac{\Gamma}{2} & 0 & 0 & -g & 0 & 0 & 0 & 0 \\ \frac{\kappa}{2} & \frac{\Gamma}{2} & 0 & 0 & 0 & 0 & \varepsilon & 0 & 0 \\ 0 & 0 & 0 & -(\frac{\Gamma}{2} + \frac{\kappa}{2}) & -(\omega_0 - \omega_c) & 0 & 0 & 0 & -\varepsilon \\ g & -g & 0 & (\omega_0 - \omega_c) & -(\frac{\Gamma}{2} + \frac{\kappa}{2}) & 0 & 0 & -\varepsilon & 0 \\ 0 & 0 & 0 & 0 & 0 & -\frac{\kappa}{2} & (\omega_c - \omega_l) & 0 & g \\ \varepsilon & 0 & -\varepsilon & 0 & 0 & -(\omega_c - \omega_l) & -\frac{\kappa}{2} & -g & 0 \\ 0 & 0 & 0 & 0 & \varepsilon & 0 & g & -\frac{\Gamma}{2} & (\omega_0 - \omega_l) \\ 0 & 0 & 0 & \varepsilon & 0 & -g & 0 & -(\omega_0 - \omega_l) & -\frac{\Gamma}{2} \end{pmatrix} \cdot \begin{pmatrix} R_{11} \\ R_{22} \\ R_{33} \\ R_{12} \\ I_{12} \\ R_{13} \\ I_{13} \\ R_{23} \\ I_{23} \end{pmatrix} = \begin{pmatrix} 0 \\ 0 \\ 0 \\ 0 \\ 0 \\ 0 \\ 0 \\ 0 \\ 0 \end{pmatrix}$$

This system was solved with the help of a mathematics program. The resulting expressions are long and contain different combinations of the matrix coefficients. We do not write them down here. In the next step all terms which contain ε in a higher than first order are consequently neglected.

To obtain the populations of atom and cavity we need only R_{11} , R_{22} and R_{33} . We see that in our approximation $R_{11}, R_{22} \ll R_{33}$, thus we can norm the density matrix by setting $\rho_{11} = \frac{R_{11}}{R_{33}}$ and $\rho_{22} = \frac{R_{22}}{R_{33}}$.

The result is then:

$$\rho_{11} = \frac{\varepsilon^2 \left(\frac{\Gamma^2}{4} + \omega_l^2 \right)}{\omega_l^4 - 2\omega_c \omega_l^3 + \left(\left(\frac{\kappa^2}{4} + \frac{\Gamma^2}{4} - 2g^2 \right) + \omega_c^2 \right) \omega_l^2 + 2(g^2 - \frac{\Gamma^2}{4}) \omega_c \omega_l + \left(\left(\frac{\kappa\Gamma}{4} + g^2 \right)^2 + \frac{\Gamma^2}{4} \omega_c^2 \right)}$$

$$\rho_{22} = \frac{\varepsilon^2 g^2}{\omega_l^4 - 2\omega_c \omega_l^3 + \left(\left(\frac{\kappa^2}{4} + \frac{\Gamma^2}{4} - 2g^2 \right) + \omega_c^2 \right) \omega_l^2 + 2(g^2 - \frac{\Gamma^2}{4}) \omega_c \omega_l + \left(\left(\frac{\kappa\Gamma}{4} + g^2 \right)^2 + \frac{\Gamma^2}{4} \omega_c^2 \right)}$$

This result is valid in the weak-field limit, i.e. the driving field ε must be so weak, that both populations are well below 1.

Bibliography

- [Mir02] Y. Miroshnychenko: “*Design and test of an optical high finesse resonator for single atom experiments*”, diploma thesis at University of Bonn, 2002
- [Car93] H. Carmichael, “*An open systems approach to quantum optics*”, Springer 1993
- [Sch01] D. Schrader, S. Kuhr, W. Alt, M. Mueller, V. Gomer and D. Meschede, “*An optical conveyor belt for single neutral atoms*”, Appl. Phys. B 73(8), p. 819 (2001)
- [Kuhr01] S. Kuhr, W. Alt, D. Schrader, M. Müller, V. Gomer and D. Meschede, “*Deterministic delivery of a single atom*”, Science **293**, 278
- [Kuhr03] S. Kuhr, “*A controlled quantum system of individual neutral atoms*”, dissertation at University of Bonn, 2003
- [Dot02] I. Dotsenko: “*Raman spectroscopy of single atoms*”, diploma thesis at University of Bonn, 2002
- [Jay63] E. Jaynes and F. Cummings, Proc. IEEE 51. p. 89 (1963)
- [Sie86] A. Siegman, “*Lasers*”, University Science Books, California (1986)
- [Shor94] P.W. Shor, “*Discrete logarithms and factoring*”, Proc. 35th Annual Symp. on Foundations of Computer Science, Nov. 1994, pp. 124-134
- [Dre83] R. Drever and J. Hall, “*Laser phase and frequency stabilization using an optical resonator*”, Appl. Phys. B 31, p. 97 (1983)
- [Tan02] Sze M. Tan: “*Quantum optics and computation toolbox for Matlab*”
- [Ste98] D. A. Steck: “*Cesium D Line Data*”
- [Sho90] B. W. Shore: “*The theory of coherent atomic excitation*”, vol. 1, Wiley 1990
- [Scu97] M. O. Scully, M. S. Zubairy: “*Quantum optics*”, Cambridge university press, 1997
- [Osn01] S. Osnagi, P. Bertet, A. Auffeves, P. Maioli, J.M. Raimond and S. Haroche: “*Coherent control of an atomic collision in a cavity*”

- [Lieb03] D. Liebfried, R. Blatt, C. Monroe, D. Wineland, “*Quantum dynamics of single trapped ions*”, *Reviews of Modern Physics*, V. 75, Jan. 2003
- [Yi02] X. X. Yi, X. H. Su and L. You: “*A conditional quantum phase gate between two 3-state atoms*”, quant/ph 0210160

Acknowledgements

The year of my diploma work is now over and I want to thank all the people who helped and supported me during this time. I want to thank

the “single-atoms” team, in particular:

Dominik Schrader for teaching me all things I needed in the lab and forgiving even my most stupid mistakes,

Wolfgang Alt for being able to answer all my questions, showing new ways when I was stuck, and his endless patience with me,

Dr. Stefan Kuhr for his endless energy and optimism, even during night measurements,

Yevhen Miroshnychenko and Igor Dotsenko for their help in my work and nice time spent together,

Mika Khudaverdyan for punching me every time I was about to lose my sense of humor, these people work hard and enthusiastic on this complex and fascinating experiment;

all other members of the group for the friendly atmosphere,

Prof. Dr. D. Meschede for providing me access to all this,

Prof. Dr. K. Buse for being my coreferent,

my parents for their endless love and support,

my sensei Jury Jukelis for sharing his strength with me,

and Julia Mark for dreaming the Venice dream with me.

Thank you!

Wenjamin Rosenfeld, August 2003